JOURNAL OF GEOPHYSICAL RESEARCH, VOL. 100, NO. E7, PAGES 14,361–14,381, JULY 25, 1995

Determining heights and slopes of fault scarps and other surfaces on Venus using Magellan stereo radar

Chris Connors

Department of Geological and Geophysical Sciences, Princeton University, Princeton, New Jersey

Abstract. This report presents relationships and techniques for determining the heights and slopes of discretely dipping surfaces, such as normal fault scarps, on the surface of Venus from measurements of their widths in Magellan stereo synthetic aperture radar (SAR) images. These surfaces are clearly recognizable as distinct bands of increased or decreased radar backscatter relative to flat-lying areas in the 120 to 280-m resolution Magellan SAR images, but are not generally imaged in the >10-km resolution Magellan altimetry. Our methods take into account radar distortion effects, and allow one to determine whether a slope is foreshortened, laid over, elongated, or in radar shadow. The techniques make use of graphs constructed for the Magellan incidence angle profiles so that investigators can determine the local height and slope of an individual surface in a straightforward manner, but the techniques are applicable to any stereo radar data set if the radar incidence angles are known. Additionally, the techniques can be used to improve digital elevation models constructed using radar stereoscopy in areas that have steep local terrain where stereoscopic fusion may be impossible due to the effects of layover or radar shadow. Using these techniques we show that there are normal fault scarps on Venus with heights in the 700-m range that have remarkable topographic slopes of close to 60°, something unheard of on Earth and which suggests a high effective cohesive strength of the Venusian crust.

Introduction

The surface expression of faults and folds on Earth varies tremendously due to erosion, deposition and subsequent deformation. These modifications result in surface morphologies only indirectly indicative of quantitative deformational geometries such as fault slip or fold amplitude. In contrast, Venus is a planet whose surface has undergone little large-scale erosion. This is mainly due to a lack of water in the atmosphere and on the surface of Venus [*Kaula*, 1990]. Water on Earth contributes to erosion through the facilitation of physical and chemical weathering, and transport of material. Although minor eolian processes [*Ardvidson et al.,* 1992; *Greeley et al.,* 1992] and modest chemical weathering [*Klose et al.*, 1992] have been recognized, the principal ways in which structures can be modified on the surface of Venus are through flooding by lava flows [*Head et al.*, 1992], landslides [*Malin*, 1992], and further deformation.

These modifications on Venus are minor in comparison to those acting on Earth, and as a result, the geomorphology of deformed areas on Venus closely reflects underlying structural geometries. Venus thus offers a unique opportunity to study map-scale structures in a nearly unaltered state. Because of this strong association of topography and structural geometry, quantitative measures of surface shape should thus be extremely useful in interpreting the underlying causative structural elements on Venus.

The highest resolution images of Venus are Magellan synthetic aperture radar (SAR) data. Because of its 120 to 280-m range resolution [*Pettengill et al.,* 1991] and because SAR highlights topography, map-scale compressive folds and normal faults are some of the most striking geologic features on the surface of Venus imaged by Magellan SAR (Figure 1). However, a SAR image by itself does not provide quantitative topographic information. To extract topographic information of structures imaged with SAR requires a full account of the distortions inherent in SAR, which is the purpose of this paper.

Paper number 95JE01134.
0148-0227/95/95JE-01134$05.00

Limitations of Current Topography of Venus

The highest quality global topographic data for Venus are Magellan altimetry gridded to 4.6 km/pixel horizontal resolution. However, this is resampled from Magellan altimetric echoes, which have footprint resolutions generally greater than 10 km in both the azimuth and range directions [*Pettengill et al.,* 1991]. In general, Magellan altimetry provides the broad topographic information of the surface, but does not have high enough horizontal resolution for the determination of slopes and heights of individual fault scarps, scree slopes, or fold limbs. For example, altimetric contour lines trend across faces in Figure 1 which must have topographic relief because they are observable in the SAR image as linear features with distinctly different radar backscatter.

Preliminary studies have been conducted to develop higher resolution topographic data sets using Magellan data. *Ford and Pettengill* [1992] showed that Magellan altimetry can be reprocessed to yield an approximately 2 km/pixel horizontal resolution. This resolution, however, is only possible near periapsis and is still probably too coarse to resolve all but the largest folds and faults on Venus. The combined use of altimetric power-versus-time echoes and SAR is a promising way of determining heights and slopes of individual scarps on Venus. Although later we show an example that makes use of altimetric echoes, full treatment of this technique is beyond the scope of this paper.

Leberl et al. [1992] used equivalent point determination by stereoscopic fusing of cycle 1 and cycle 2 stereo SAR image pairs

Figure 1. Magellan cycle 1 SAR image located at about 30°S, 142°. The northwest trending bright and dark features are probably fault scarps or scree slopes associated with normal faulting that have discrete dips relative to other areas in the image. Those discretely dipping surfaces facing toward the antenna are visible as areas with high radar backscatter (brighter than average in the image), whereas surfaces facing away from the antenna can be recognized by their low backscatter (darker than average). Magellan altimetry is superimposed as contours in meters above 6051-km planetary radius. Because of the much lower resolution of Magellan altimetry, there is poor correlation between altimetry and individual discretely dipping surfaces in the SAR image.

to generate digital elevation models (DEMs) with approximately 100-m topographic resolution. With the same technique, the Magellan Stereo Toolkit (Vexcel Corporation, Boulder, Colorado) can be used to construct DEMs using the cycle 1-cycle 3 stereo data set. This technique of extracting topographic information from radar parallax is probably the most promising for the generation of high-resolution topography over broad areas of Venus, but requires the use of some sort of stereoplotter, such as the Magellan Stereo Toolkit, or other stereo-mensuration device such as a parallax bar. In addition, in many regions with steep local terrain the effect of radar layover and, to a lesser extent radar shadow, will, if present, make it impossible to stereoscopically fuse steep slopes. Radar layover is the geometric distortion in which the base and crest of a slope in a radar image are reversed relative to their true positions on the surface (Figure 4b). This occurs when the incidence angle of the radar beam (Figure 2a) is less than the topographic slope.

Some initial work has attempted to address the layover problem. *Leberl* [1990] gave a solution for the height of a vertical feature that was laid over. *Wu* [1982] presented a solution for the height of an object that is laid over in two side-looking airborne radar images with different viewing geometries by using the slant range and radar station position. *Ford and Pettengill* [1992] applied a similar technique by using the slant range and distance from the spacecraft nadir to solve for the height and slope of laid-over features in Magellan cycle 1 and cycle 2 stereo SAR images.

Layover is not generally a problem in extracting topographic data from stereo side-looking airborne radar (SLAR) on Earth because the large incidence angles used in SLAR [see *Leberl*, 1990] greatly decrease the occurrences of topographic slopes being greater than the incidence angle. However, layover is a significant problem in Magellan SAR because, like most satellite-based SAR, incidence angles are much smaller than SLAR (Figure 2a). We explore the phenomena of radar layover in more detail in the section on radar distortions.

The methods described below are an attempt to simplify the extraction of topographic information of discretely imaged surfaces on Venus by using the standard cycle 1 and cycle 3 mosaicked image data records (MIDRs) and Magellan SAR incidence angles. The methods allow interpreters to determine whether a surface is foreshortened or laid over, elongated or in radar shadow, and to quantify heights and slopes without the use of elaborate stereo equipment. They can be used by scientists in a straightforward manner for qualitative and quantitative analyses of distinct surfaces that are imaged with Magellan stereo SAR, but are not adequately sampled with Magellan altimetry. These techniques can also be used to augment radar-stereo DEM generation. Although the techniques are applied to Magellan SAR, they are applicable to any stereo-radar data set, in particular, other satellite-based SAR systems such as the Shuttle imaging radar and the soon-to-be-operating Canadian Radarsat satellite.

Magellan SAR

SAR was collected during three "cycles" of the Magellan mission. Each cycle corresponded to one rotation of Venus about its axis (equivalent to a little over 243 Earth days). Cycle 1 and cycle 3 SAR images are said to be "left looking" because the antenna transmitted and received microwave energy to the left of the imaged surface (Figure 2a), whereas cycle 2 Magellan SAR images are "right looking" with energy transmitted and received to the right of the imaged surface. There was also a small amount of SAR collected in cycle 2 that was left looking, but in this report, cycle 2 images will always refer to right-looking SAR.

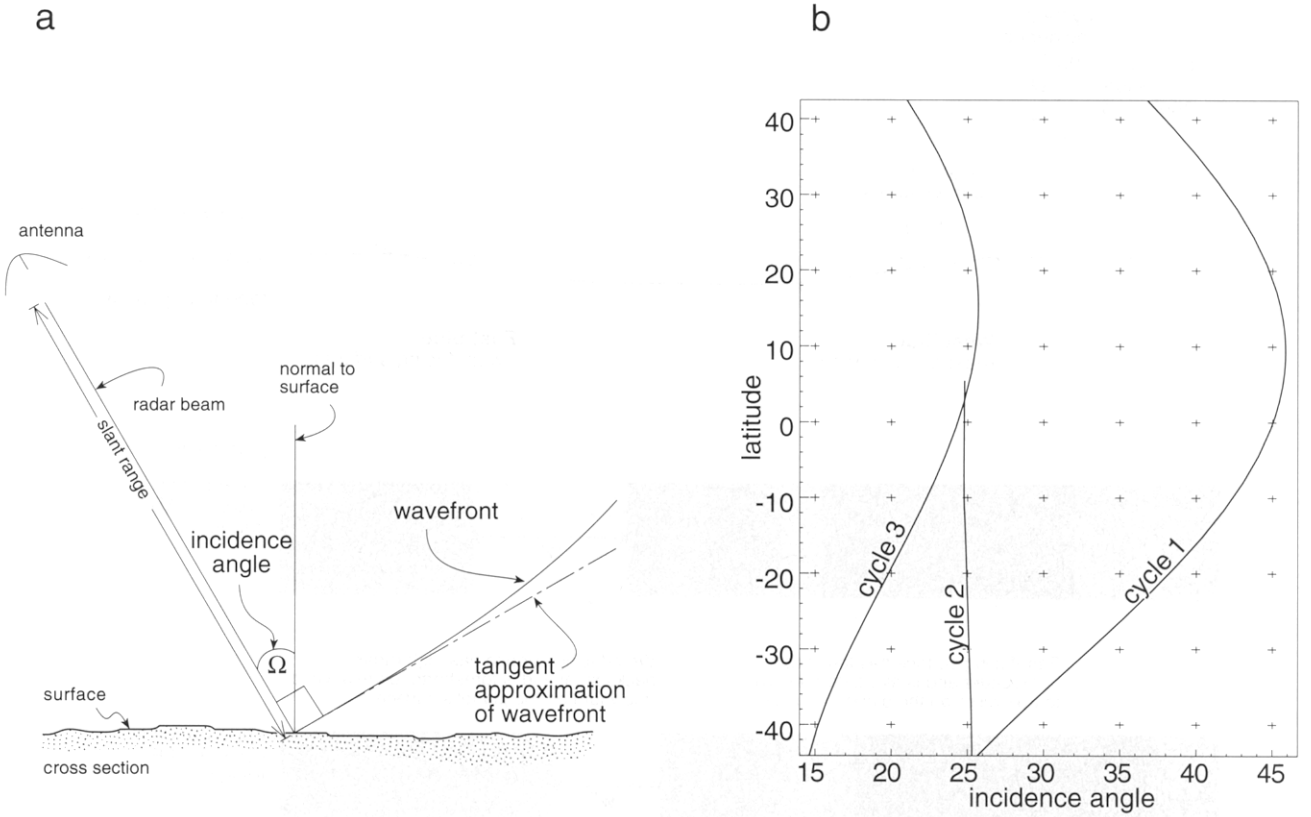

Figure 2. (a) Geometry and nomenclature of a SAR sensor. (b) Incidence angles with respect to latitude for cycle 1, 2, and 3 Magellan SAR from orbits 1199 (for cycle 1), 3049 (cycle 2), and 4800 (cycle 3). These incidence angle profiles are representative of the vast majority of stereo coverage for Magellan from 60° to 180°E longitude, and can probably be used for all cycle 1-cycle 3 stereo SAR except for images around Maxwell Montes where a different stereo geometry was used.

Recognizing Discretely Dipping Surfaces in Magellan Radar

Because cycle 1 and cycle 3 SAR images look left as the spacecraft travels from north to south in an orbit, the surface is illuminated from the west. This results in distinctive radar signatures in the images for different discretely dipping surfaces on Venus because radar backscatter increases as the local incidence angle (i.e., the angle between the radar beam and the normal to the local surface) decreases [*Muhleman*, 1964]. Consider the schematic topographic trough illuminated from the left, shown in cross section at the top of Figure 3. The trough strikes parallel to the path of the satellite (along track direction). The appearance of the trough in cycle 1 and cycle 3 SAR images is shown in the bottom of Figure 3.

The east side of the trough is a discretely dipping west facing surface that will display higher backscatter in the radar image because this slope faces toward the antenna and thus scatters more energy in the direction of the antenna. This higher backscatter will generally appear distinctly brighter than nearby horizontal areas in the images. Likewise, the west side of the trough will have lower backscatter and appear dark in radar images because it faces to the east, away from the antenna. For example, the bright linear features in the cycle 1 SAR image of Figure 1 mostly represent surfaces dipping to the west, whereas the dark linear features are generally surfaces dipping to the east.

Because cycle 2 Magellan SAR is right-looking, the surface is illuminated from the east. Thus the appearance of the topographic trough of Figure 3 will be reversed from that in the left-looking cycle 1 and 3 SAR. West facing surfaces will display lower backscatter and appear darker; east facing surfaces will display higher backscatter and appear brighter in cycle 2 images.

The orientation of the surface is not the only contributor to radar backscatter. High surface roughness (particularly at low latitudes on Venus where Magellan incidence angles are largest) or high dielectric constant (particularly at very high elevations on Venus) can dominate over surface slope differences in the radar signature [*Pettengill et al.*, 1991]. For structural studies these effects do not generally inhibit the determination of discretely dipping features because laterally extensive linear features can usually be distinguished from more irregularly shaped features that may be rough or have high dielectric constants. The one exception is probably the ejecta of most impact craters. These ejecta are generally so rough that it is often difficult to detect discretely dipping surfaces in these features from radar backscatter alone.

Thus, through a cursory examination of the brightness of a feature in a SAR image, we conclude that we can often qualitatively determine whether a surface dips to the west (brighter in cycle 1 and 3 images, darker in cycle 2 images) or dips to the east (darker in cycle 1 and 3 images, brighter in cycle 2 images). However, we require an understanding of the distortions present in radar in order to extract quantitative slope and height information from the images.

Radar Distortions

Synthetic aperture radar, such as Magellan's, measures time delay (slant range) of a returned pulse in a side-looking mode.

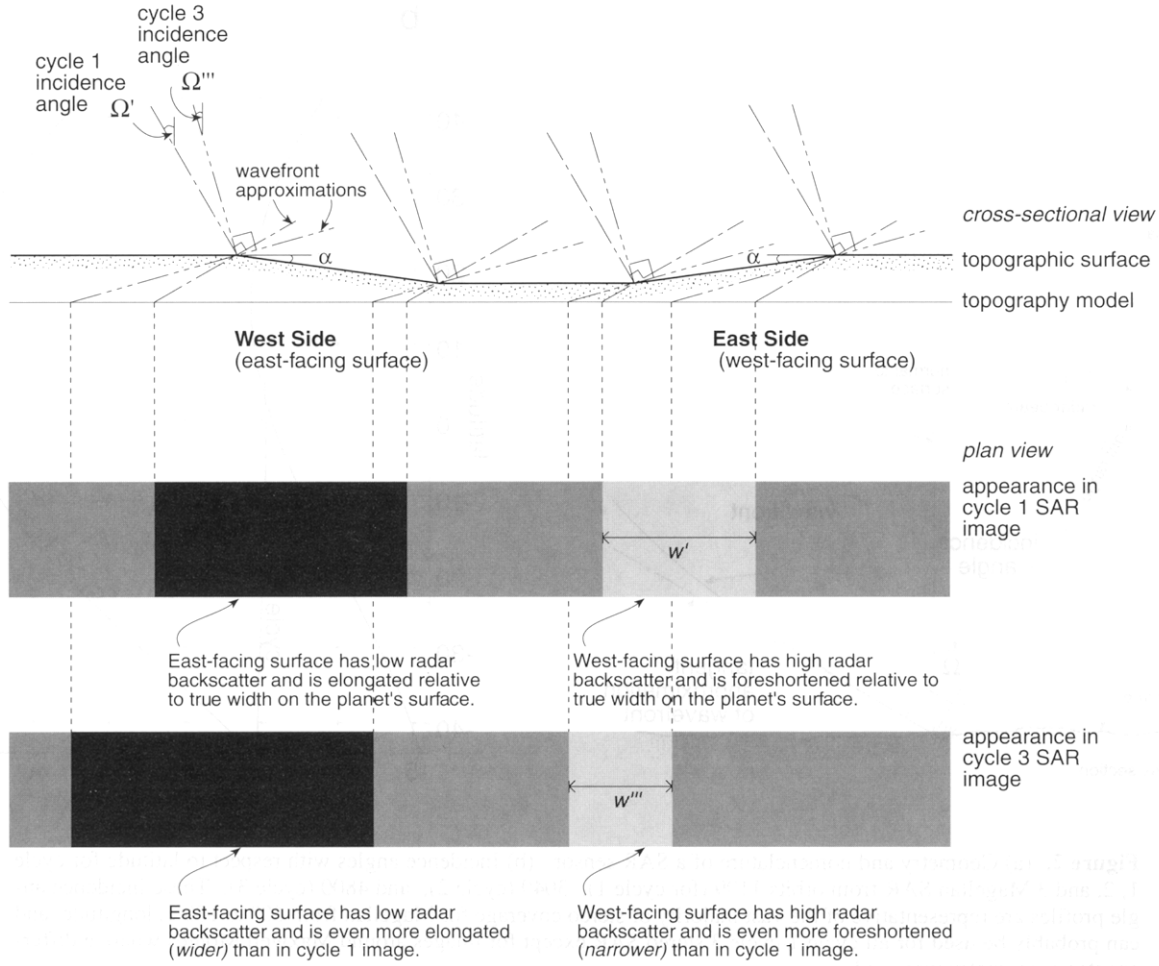

Figure 3. Shown are the expected ground range in left-looking cycle 1 and cycle 3 Magellan SAR images of a symmetric topographic trough striking parallel to the azimuth direction (the direction the antenna is moving as SAR is collected). The west facing surfaces display higher radar backscatter because more energy is returned to the antenna than in the flat-lying areas around the trough, while the east facing surfaces display lower backscatter. Because of radar distortions (see Figure 4) the appearance of the trough is not symmetric.

The energy returned is projected or mapped onto a low-resolution (>26 km/pixel horizontal resolution) model of topography in the ground range presentation. As a result, objects with topographic relief will be displaced from their true positions on the planet's surface because features standing higher than this topography model will be detected sooner than features with the same height as the topography model. For example, the crest of the topographic trough in Figure 3 is displaced toward the antenna more than the base of the trough. In left-looking cycle 1 and 3 images these displacements are toward the west, and in cycle 2 images they are toward the east. These distortions are in the opposite sense to that of aerial photography, where objects are displaced away from the nadir point of the photo.

Unless the topography model is of the same resolution as the SAR, these distortions will always be present. These changes in the apparent positions of objects with relief are the fundamental artifacts that must be kept in mind when conducting geologic analyses of any SAR images, and we discuss them in detail below with respect to the particular geometry of Magellan SAR.

Modeling the circular wave front of the radar as its tangent (Figure 2a), we can closely approximate the positions of features with relief in Magellan SAR (Figure 3). This approximation is common in radar analysis, including that by *Leberl et al.* [1992] for Magellan radar stereoscopic studies. The tangent approximation is valid because the slant range distance in Magellan SAR is from 425 to 2196 km [*Pettengill et al.,* 1991], and thus the difference in the position of a feature between using a circular wave front and its tangent is very small. For example, for a feature 1 km above the topography model, this difference varies from 6 to 18 m in Magellan radar images. Thus the mapping of this wave front approximation onto the topography model will closely approximate the position of the feature in the SAR image detected at that range.

The height of the topography model used in the processing of most Magellan SAR is primarily based on Pioneer Venus altimetry. These values vary over large distances, but because the resolution of the topography model is >26 km/pixel, the topography model approximates a plane at the scale of the structures we are concerned with in this report, such as the individual fault scarps and scree slopes shown in Figure 1 and in other figures.

In the trough of Figure 3 we use a topography model with a lower elevation than all features of the trough, although in actual images, the elevation of the topography model may be greater or less than the elevation of the individual topographic features. In

the next section, where we derive the relationships of the widths of a discretely dipping face in the images to the face's height and slope, we use a topography model that is arbitrarily placed at the base of the face, for geometric convenience. We will show later in the discussion of radar parallax that a knowledge of elevations of the topography model is not necessary for relative height and slope determinations, providing the real topography model approximates a horizontal plane. Exact elevations of the topography model are only required for absolute elevation determinations.

Foreshortening of the Image of a Surface

We concluded in a previous section that we can recognize discretely dipping surfaces, such as normal fault scarps, based on their radar backscatter intensity. Because of the distortion effects of features with topographic relief, the width of the band of increased radar backscatter due to a slope facing the antenna, such as a west facing slope in cycle 1 and 3 SAR or an east facing slope in cycle 2 SAR, will become foreshortened in the near-range direction (toward the antenna) relative to its true width. That is, the width of the face in the images will always be less than the face's horizontal extent on the planet's surface. We see from Figure 4a that the width, w, of this band of increased brightness for a foreshortened face can be given by

$$w = \frac{h}{\tan \alpha} - \frac{h}{\tan \Omega} = \frac{h(\tan \Omega - \tan \alpha)}{\tan \Omega \tan \alpha} \quad (1)$$

where h is the height of the face from the base to the crest, α is the topographic slope in the range direction (normal to the orbit path), and Ω is the nominal incidence angle of the radar beam. The term "nominal incidence angle" is the angle between the radar beam and the normal to the topography model. We will use simply "incidence angle" in the rest of this paper to refer to this angle (Figure 2a).

Magellan radar varies in incidence angle from about 46° at periapsis (10°N latitude) to 14° at high latitudes (Figure 2b); thus the width of a face in Magellan SAR will be narrower at high latitudes on Venus (will be more foreshortened) relative to the width at low latitudes for a face with the same height and slope. Additionally, in order to optimize stereo capabilities the cycle 3 incidence angles, Ω'', are smaller than cycle 1 incidence angles, Ω', for all latitudes except in special stereo cases such as over Maxwell Montes. So foreshortening is more severe in cycle 3 images (Figure 3).

Radar Layover

If the slope of a surface that faces the antenna exceeds the incidence angle of the radar beam, that is if $\alpha > \Omega$, then the energy at the crest of the west face will arrive back to the antenna sooner than energy from the base (Figure 4b). This phenomenon, radar layover, results in the positions of the base and crest of a face being inverted relative to their true horizontal positions on the planet's surface. For example, in left-looking cycle 1 and 3 SAR the laid-over crest of a west facing scarp will appear to the left of the base of the scarp (Figure 4b). Because the cycle 1 and 3 incidence angles are different, the face may be laid over in one, both, or neither of the images. Furthermore, because of the variation of incidence angles in Magellan radar with latitude (Figure 2b), a slope that is foreshortened at low latitudes may be laid over at high latitudes. We can relate the width of a laid over face to the height and slope of the face by the same equation as for a foreshortened face (1), but solution for the width of a laid-over face will always result in a negative number. Precisely at the transition from foreshortening to layover, $\Omega = \alpha$, and thus $w = 0$.

Layover is widespread in Magellan SAR and is a particular problem in cycle 3 images because of the smaller incidence angles during this cycle. Because normal fault scarps and scree slopes may be steep enough to cause layover in Magellan SAR, those interested in fine-scale geomorphic and structural analyses on Venus must address the layover problem. The appearance of a laid-over face in Magellan SAR is similar to a foreshortened face, in that it has increased radar backscatter relative to flat-lying areas. Laid-over faces often look more diffuse in their radar character than foreshortened faces, but without images collected at multiple incidence angles, it is impossible to definitively determine whether a face is laid over or foreshortened, unless its height is independently known (see below).

Elongation of the Image of a Surface

For a slope facing away from the antenna, the width of the band of decreased radar backscatter will be larger than its true width. With decreasing incidence angle, the width of the slope in the images will be more elongated, the opposite distortion to that found in slopes facing the antenna (Figures 3 and 4c). The width, w, of this band of decreased brightness for an elongated face is

$$w = \frac{h}{\tan \alpha} + \frac{h}{\tan \Omega} = \frac{h(\tan \Omega + \tan \alpha)}{\tan \Omega \tan \alpha} \quad (2)$$

where h is the height of the face from the base to the crest; α is the topographic slope in the range direction, and Ω is the incidence angle of the radar beam. As with foreshortening and layover, this elongation will vary with latitude in Magellan SAR. For example, elongation will be greater at high latitudes in the images because Magellan SAR was collected at smaller incidence angles at high latitudes relative to low latitudes. Additionally, the elongation will be greater in cycle 3 than cycle 1 images because of the smaller incidence angles (Figure 2b).

Radar Shadow

If the slope of a surface facing away from the antenna is greater than the complement of the incidence angle, $\alpha > 90 - \Omega$, the face will not be imaged, and there will instead be a radar shadow present in the image. The width of a shadow is the minimum width observable for a given incidence angle and height of a surface facing away from the antenna. This width is shown in Figure 4d to be given by

$$w = \frac{h}{\tan \alpha} + h \tan \Omega = \frac{2h}{\sin 2\Omega} \quad (3)$$

It should be noted that we are defining height of the face in this instance as the height from the crest of the face to where the shadow impinges on the surface. Radar shadows should appear darker than an elongated face that simply slopes away from the antenna because no energy is being returned to the antenna from that part of the surface. If one has access to the digital images, and Magellan noise levels, one can theoretically determine whether or not a face is in radar shadow because a face in radar shadow will have pixel values of normalized backscatter cross section less than or equal to the Magellan noise level for that particular orbit and latitude. The most important Magellan signal-to-noise ratios can be obtained from the Magellan Notepad (available at http://delcano.mit.edu). Although radar shadows are

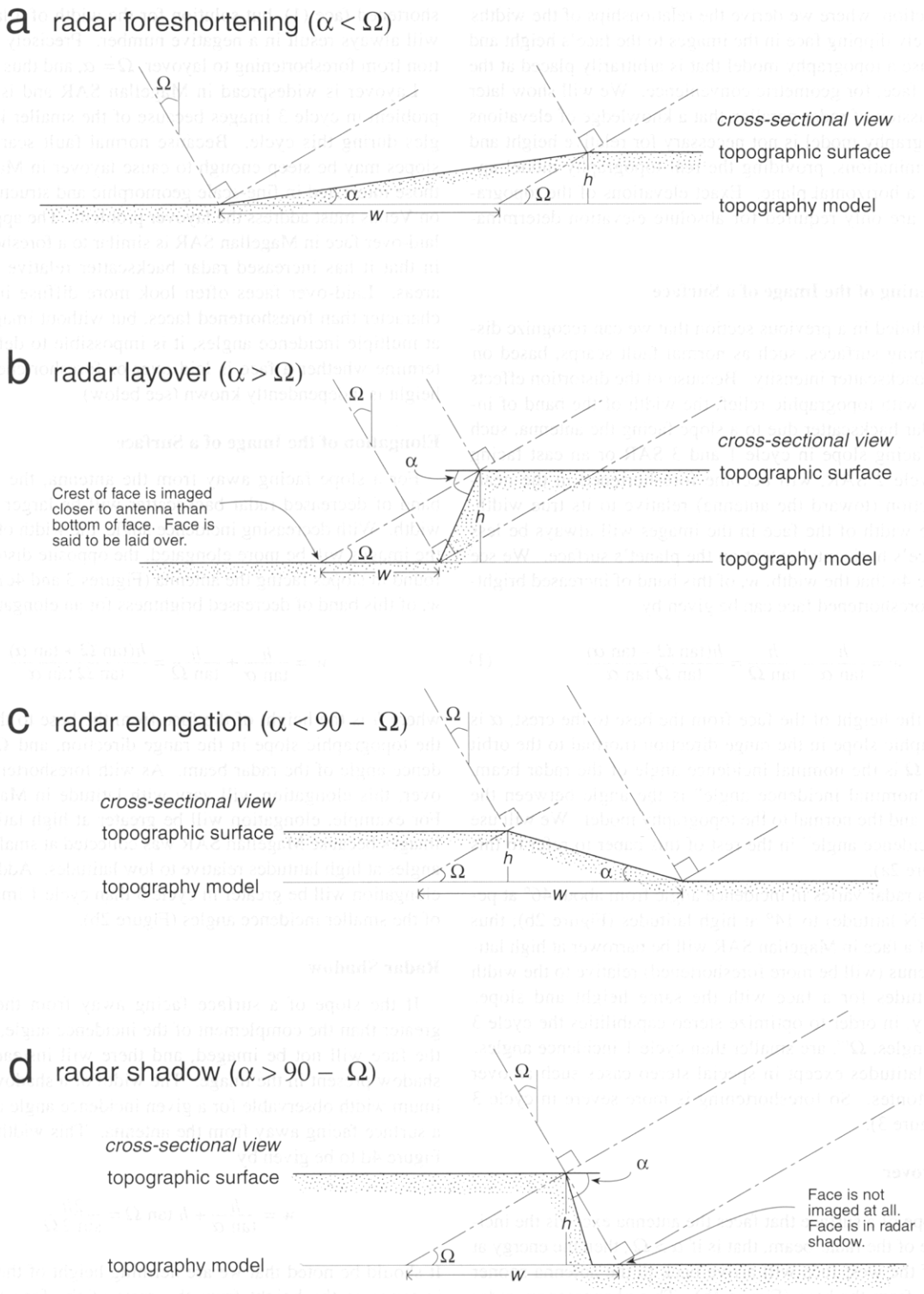

Figure 4. Geometric distortions in radar images. Shown are the relationships of the topographic slope α height h and width w of a face as seen in left-looking SAR images with an incidence angle Ω; see (1) - (3) for relations. (a) Radar foreshortening, a face that is facing toward the antenna, is narrower in a SAR image than its true width on the planet's surface. (b) Radar layover, for a face that is facing toward the antenna, the crest of the face is imaged closer to the antenna than the base of the face. The face may be narrower or wider in image than true width. (c) Radar elongation, a face that is facing away from the antenna, is wider in a SAR image than its true width on the planet's surface. (d) Radar shadow: face is not imaged at all. For a given height and incidence angle this is the minimum width of a surface facing away from the antenna.

common in SLAR images on Earth, we have observed very few in Magellan SAR. This is a function of the relatively small incidence angle range of Magellan SAR relative to SLAR, and because there seems to be fewer steep slopes on Venus than on Earth. The lack of steep slopes is probably due to a lack of water-related erosion on Venus; water-related erosion is responsible for most of the steep slopes on Earth.

Nonuniqueness of Widths in Images

The incidence angle for a Magellan SAR image can be obtained from Figure 2b, but these width relations for foreshortened, laid-over, and elongated faces still do not provide unique values for the height and slope. That is, from (1) an infinite number of pairs of heights and slopes result in the same width; a similar limitation occurs with using (2). For faces that are in radar shadow, no slope information can be extracted, but the height can, of course, be determined with (3).

We develop below simple methods that incorporate multiple width measurements from multicycle stereo radar to uniquely solve for the height and slope of a face. Because these methods relate the widths to the radar parallax of the base and crest of a face, we first address radar stereoscopy as it applies to Magellan SAR.

Radar Stereoscopy

Extracting Absolute Heights From Radar Parallax

To compute the heights of features in stereo SAR images, one measures the geometric disparities between a stereo pair [*Leberl et al.,* 1992]. Stereoscopy is difficult with opposite-side radar because of the drastic differences in the radiometric and geometric disparities of features imaged in opposite look directions. Although sophisticated processing of images may greatly lessen these disparities [*Fullerton et al.,* 1986; *Leberl,* 1990], for standard stereoscopy same-side radar is much more tractable; therefore we concentrate our analysis on left-looking cycle 1 and 3 Magellan stereo SAR. To apply the methodology to these images, consider the crest of the west face with height, h_c, in Figure 5. Recall that during cycle 1, the antenna records a time delay which is mapped onto the ground range topography model in the processing of the images, displacing the true position of the feature by p_c'. The crest is displaced a larger amount, p_c''', in the cycle 3 image because cycle 1 incidence angles are greater than cycle 3 incidence angles, $\Omega' > \Omega'''$, for all latitudes except in special stereo cases such as over Maxwell Montes. The separation in the ground range images between these positions, dp_c, is termed the parallax difference [*Leberl et al.,* 1992]. Similarly, every point along the surface with a different height above the topography model will have a unique parallax difference in the cy-

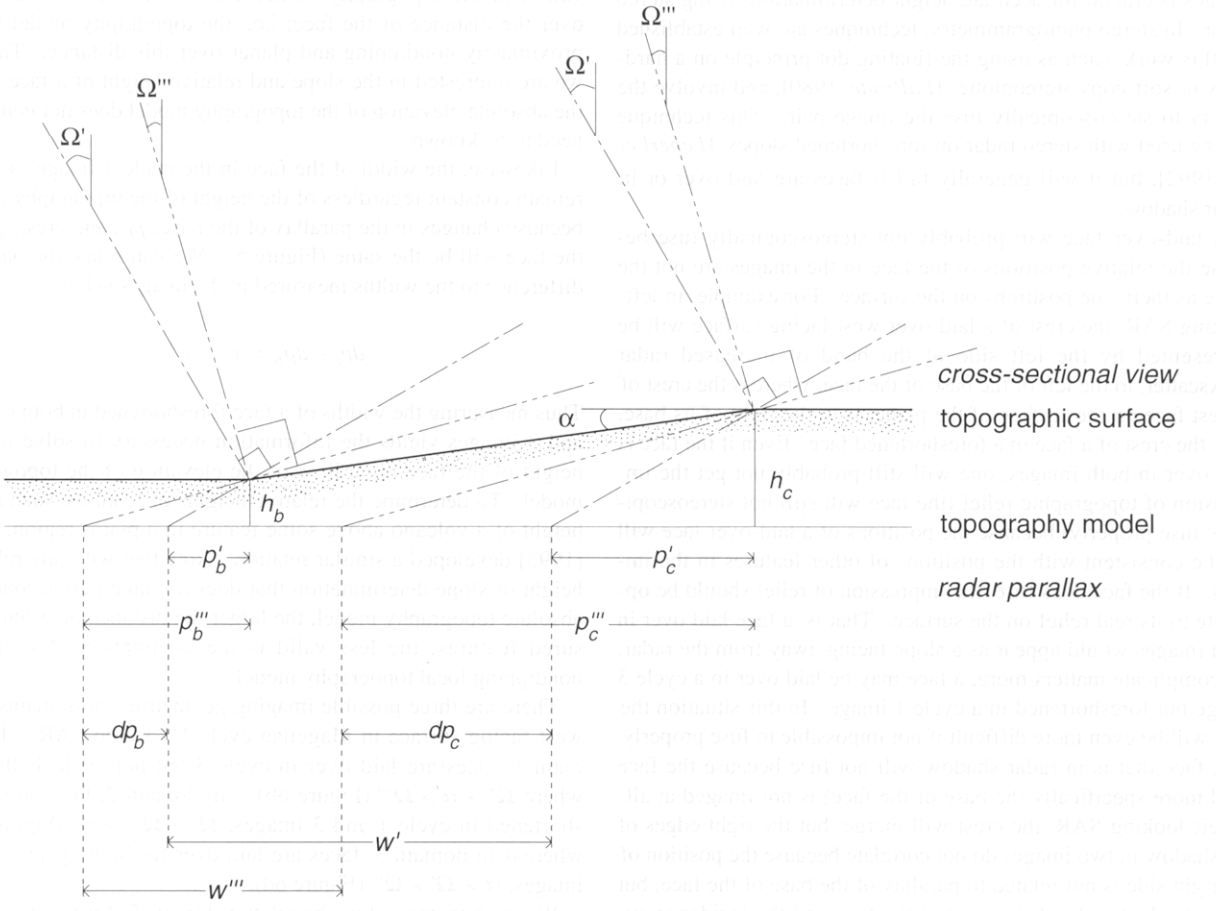

Figure 5. Displacement of features with relief relative to topography model and determination of height, h, from the parallax difference, dp. The crest of the face will have a larger parallax difference, dp_c, than the base, dp_b, because it has a larger height above the topography model.

cle 1 and 3 images. For example, the base of the face with height h_b will have the parallax difference dp_b (Figure 5).

One can solve for the height, h, of an object above the topography model through the relation of *Leberl et al.* [1992]

$$h = dp / (\cot \Omega''' - \cot \Omega') \quad (4)$$

where dp is the parallax difference (Figure 5). For the crest in Figure 5, $dp = dp_c$ and $h = h_c$. Note dp is measured in the range direction as the difference in the position of a feature in the cycle 1 and cycle 3 images relative to the graticule. Because the range direction is approximately east-west, these equivalent points will have different longitudes and, to a much lesser extent, different latitudes unless a feature has no height relative to the topography model.

To determine an absolute elevation (planetary radius), this calculated height is then added to the planetary radius of the low-resolution topography model used in the processing of the original SAR images. This technique was used successfully with Magellan cycle 1 and cycle 2 left-looking images as part of the Magellan cycle 2 stereo experiment to construct digital elevation models of selected regions [*Leberl et al.*, 1992], and is the basis of the Magellan Stereo Toolkit.

Necessity of New Methods for Steep Faces

Determining that an equivalent point has been selected on both images is crucial for accurate height determinations using stereo radar. In stereo photogrammetry, techniques are well established for this work, such as using the floating dot principle on a hard-copy or soft-copy stereoplotter [*LaPrade*, 1980], and involve the ability to stereoscopically fuse the image pair. This technique can be used with stereo radar on foreshortened slopes [*Leberl et al.*, 1992], but it will generally fail if faces are laid over or in radar shadow.

A laid-over face will probably not stereoscopically fuse because the relative positions of the face in the images are not the same as their true positions on the surface. For example, in left-looking SAR, the crest of a laid-over west facing surface will be represented by the left side of the band of increased radar backscatter, to the left of the base of the face, whereas the crest of a west face on the surface of the planet is to the right of its base, as is the crest of a face in a foreshortened face. Even if the face is laid over in both images, one will still probably not get the impression of topographic relief (the face will still not stereoscopically fuse properly) because the positions of a laid-over face will not be consistent with the positions of other features in the images. If the face does fuse, the impression of relief should be opposite to its real relief on the surface. That is, a face laid over in both images would appear as a slope facing away from the radar. To complicate matters more, a face may be laid over in a cycle 3 image but foreshortened in a cycle 1 image. In this situation the face will be even more difficult if not impossible to fuse properly.

A face that is in radar shadow will not fuse because the face (and more specifically the base of the face) is not imaged at all. In left-looking SAR, the crest will merge, but the right edges of the shadow in two images do not correlate because the position of the right side is not related to parallax of the base of the face, but rather to the height of the crest of the face and the incidence angle. It should be noted that we are defining height of the face in this instance as the height from the crest of the face to where the shadow impinges on the surface. Although the actual elevation of the surface could change from the base of the face to this location of impingement, and thus affect the derived height of the face, with same-side stereo SAR this height is all that can be determined, because it is all that is imaged.

Although radar layover and, to a much lesser extent, radar shadow introduce complexity in the imaging of west faces, in order to extract height or slope information from Magellan stereo SAR, the task is the same as with all stereo images: detecting an equivalent point in the image pair. Thus determination of an equivalent point in Magellan stereo SAR in regions with significant local relief requires new understanding of what are indeed equivalent features for a face imaged with different incidence angles. We present this from the perspective of how the widths of discretely dipping surfaces relate to the radar parallax difference.

West Facing Surfaces in Magellan SAR

Extracting Relative Heights From Cycle 1/3 Images

We can show from (4) that $h_c - h_b \propto dp_c - dp_b$, where, $h_c - h_b$, is the height of the face from the base to the crest and $dp_c - dp_b$ is the difference between the parallax difference of the crest and base of the face (Figure 5). The parallax differences will change for the crest and base of the face, depending on the elevation of the topography model because the heights of these features relative to the topography model will be different, but the changes in the parallax difference of these features will be the same. That is, $dp_c - dp_b$ will remain the same, provided the elevation of the topography model does not change dramatically over the distance of the face; i.e., the topography model is approximately nondipping and planar over this distance. Thus, if we are interested in the slope and relative height of a face itself, the absolute elevation of the topography model does not generally need to be known.

Likewise, the width of the face in the cycle 1 image, w', will remain constant regardless of the height of the topography model because changes in the parallax of the base, p'_b, and crest, p'_c, of the face will be the same (Figure 5). We can relate the parallax difference to the widths measured in the images using

$$dp_c - dp_b = w' - w''' \quad (5)$$

Thus measuring the widths of a face foreshortened in both cycle 1 and 3 images yields the information necessary to solve for the height of the face regardless of the elevation of the topography model. To determine the relative heights of features, such as the height of a volcano above some feature in a plains region, *Plaut* [1993] developed a similar relation. Note that with any relative height or slope determination that does not take into account the absolute topography model, the larger the distance between measured features, the less valid is the assumption of a planar, nondipping local topography model.

There are three possible imaging geometries, or domains, of a west facing surface in Magellan cycle 1/3 stereo SAR. In domain 1, faces are laid over in cycle 3 but not cycle 1, that is, where $\Omega' > \alpha > \Omega'''$ (Figure 6b). In domain 2, faces are foreshortened in cycle 1 and 3 images, $\Omega' > \Omega''' > \alpha$ (Figure 6c), whereas in domain 3, faces are laid over for both cycle 1 and 3 images, $\alpha > \Omega' > \Omega'''$ (Figure 6d).

We wish to generalize the relationship of (5) for the three possible domains to determine the height, h, of a west face by expressing $dp = dp_c - dp_b$ in terms of the measurable widths in the images. Recall that from (1) for foreshortened faces ($\Omega > \alpha$) the width $w > 0$ and that $w < 0$ for laid-over faces ($\Omega < \alpha$). When

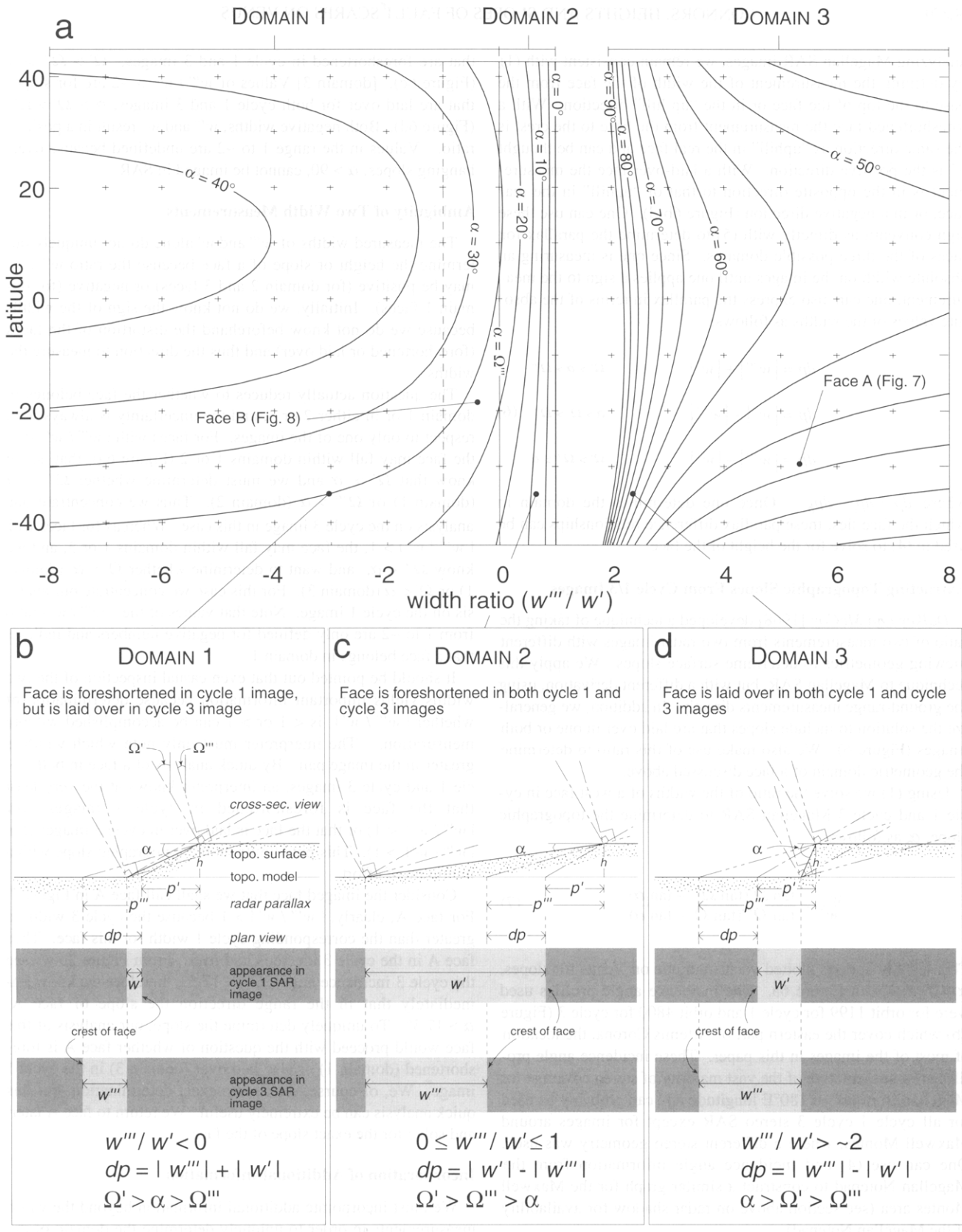

Figure 6. a) Plot of (7) for determination of the topographic slope, α , of a west facing surface from ratio of the widths, w''' / w', imaged in cycle 1 and cycle 3 Magellan SAR. Because incidence angles change with latitude in Magellan SAR (see Figure 2b), the ratio of the widths, w''' / w', is plotted versus Venusian latitude. b-d) Determination of the relative height, h, of a west facing surface from differences in the widths of the face with differing slopes in cycle 1 and 3 images. The height, h, is the same for the three faces shown, and thus the parallax difference, dp, is the same for all three. However, because the slopes of the faces vary, the widths of the faces as seen in the cycle 1 and 3 images will vary. Using the relevant width difference relationship, depending on the domain of the face, still allows one to determine the parallax difference (6) and thus the height of the face using (4).

analyzing Magellan SAR images, we remain consistent with (1) by defining the measurement of the width of the face from the base to the top of the face or in the "up hill" direction. With a foreshortened face the measurement from the base to the crest is the same direction as "uphill" in the real face and can be thought of as the positive direction. With a laid-over face the measurement is in the opposite direction to that of "uphill" in the real face, or in a negative direction (Figure 6b-d). One can use these sign conventions directly with (5) to determine the parallax for faces of the three possible domains. Since one is measuring an absolute width on the images until one applies a sign to the measurement, one can also express the parallax in terms of the absolute values of the widths as follows:

$$dp = |w'''| + |w'| \qquad \Omega' > \alpha > \Omega'''$$

$$dp = |w'| - |w'''| \qquad \alpha > \Omega' > \Omega''' \quad (6)$$

$$dp = |w'''| - |w'| \qquad \Omega' > \Omega''' > \alpha$$

where $dp = dp_c - dp_b$. Once one determines the domain in which the face lies, these parallax difference relationships can be used in (4) to solve for the height of the face.

Extracting Topographic Slopes From Cycle 1/3 Images

Dalkey and McCoy [1968] developed a technique of taking the ratio of two measurements from two radar images with different viewing geometries to determine surface slopes. We apply this technique to Magellan SAR, but with a different derivation, using the ground-range measurements directly. In addition, we generalize the solution to include slopes that are laid over in one or both images (Figure 6). We also make use of this ratio to determine the geometric domain of a face discussed above.

Using (1) we solve the ratio of the widths of a west face in cycle 1 and cycle 3 Magellan SAR to determine the topographic slope, α, as follows:

$$\frac{w'''}{w'} = \frac{\tan\Omega'(\tan\Omega''' - \tan\alpha)}{\tan\Omega'''(\tan\Omega' - \tan\alpha)} \quad (7)$$

This w'''/w' ratio is plotted versus latitude on Venus for slopes, $\alpha = 0°$ to 90° in Figure 6a. The incidence angle profiles used were for orbit 1199 for cycle 1 and orbit 4800 for cycle 3 (Figure 2b) which cover the eastern part of Artemis Corona, the location of most of the images in this paper. These incidence angle profiles are representative of the vast majority of stereo coverage for Magellan from 60° to 180°E longitude and can probably be used for all cycle 1-cycle 3 stereo SAR except for images around Maxwell Montes, where a different stereo geometry was used. One can use (4) and incidence angle information from the Magellan Notepad to construct a similar graph for the Maxwell Montes area (see section above on radar shadow for availability of the Magellan Notepad).

There are three distinct domains in the plot, which represent the three possible imaging geometries of a west face; these are equivalent to the domains discussed above for determining the height of a face. [domain 1] Values of $w'''/w' < 0$ represent faces that are laid over in cycle 3 but not cycle 1 (i.e., where $\Omega' > \alpha > \Omega'''$; Figure 6b). The negative value results from the width in the cycle 3 image, w''', being negative when laid over (1). [domain 2] Values of w'''/w' from 0 to 1 represent faces that are foreshortened in cycle 1 and 3 images, $\Omega' > \Omega''' > \alpha$ (Figure 6c). [domain 3] Values of $w'''/w' > \sim 2$ are for slopes that are laid over for both cycle 1 and 3 images, $\alpha > \Omega' > \Omega'''$ (Figure 6d). Both negative widths, w''' and w', result in a positive ratio. Values in the range 1 to ~2 are undefined because overhanging slopes, $\alpha > 90$, cannot be imaged in SAR.

Ambiguity of Two Width Measurements

The measured widths of w''' and w' alone do not uniquely determine the height or slope of a face because the ratio w'''/w' may be positive (for domain 2 and 3 faces) or negative (for domain 1 faces). Initially, we do not know the sign of the widths because we do not know beforehand the distortion of the faces (foreshortened or laid over) and thus the direction to measure the widths.

The question actually reduces to whether the face belongs in domain 1 or in either 2 or 3, and the uncertainty is always with respect to only one of the images. For faces with $|w'''/w'| < 1$, the face may fall within domains 1 or 2 (Figure 6a); that is, we know that $\Omega' > \alpha$ and we must determine whether $\Omega''' < \alpha$ (domain 1) or $\Omega''' > \alpha$ (domain 2). Thus we concentrate our analysis on the cycle 3 image in this case. Whereas for faces with $|w'''/w'| > 1$, the face may fall within domains 1 or 3, and we know $\Omega''' < \alpha$, and want to determine whether $\Omega' > \alpha$ (domain 1) or $\Omega' < \alpha$ (domain 3). For this case we concentrate our analysis on the cycle 1 image. Note that values of the $|w'''/w'|$ ratio from 1 to ~2 are only defined for negative numbers and indicate that a face belongs in domain 1.

It should be pointed out that even casual inspection of the two widths yields important information because determination of whether $|w'''/w'|$ is < 1 or > 1 can be accomplished without mensuration. The interpreter must only note which width is greater in the image pair. By quick analysis of a face in both cycle 1 and cycle 3 images, an interpreter knows at the very least that the face is foreshortened in cycle 1 images (for $|w'''/w'| < 1$) or that the face is laid over in cycle 3 images (for $|w'''/w'| > 1$). This puts limits on the topographic slope with a minimum of effort.

Consider the imaged face that we shall call face A in Figure 7. For face A, clearly, $|w'''/w'| > 1$ because the cycle 3 width is greater than the corresponding cycle 1 width for this face. Thus face A in the cycle 3 image is laid over. From Figure 2b we see the cycle 3 incidence angle, $\Omega''' = 17.5°$; therefore we know immediately that in the range direction the slope of face A, $\alpha > 17.5°$. To uniquely determine the slope, our analysis of this face would proceed with the question of whether face A is foreshortened (domain 1) or also laid over (domain 3) in the cycle 1 image. We, of course, seek more exact determination, but this quick analysis can be extremely useful. We return to face A later, and solve for the exact slope of the face.

Incorporation of Additional Information

We must incorporate additional information beyond the width measurements in order to uniquely determine the domain of the face and thus the actual height and slope of a discretely dipping west facing surface. This can take the form of (1) an additional width measurement from a cycle 2 image, (2) Magellan altimetric measurements from power-versus-time delay echoes, or (3) a consideration of the stereoscopic impression of the face or features around the face. We will concentrate on the cycle 2 measurements here, but will briefly describe the other two methods later.

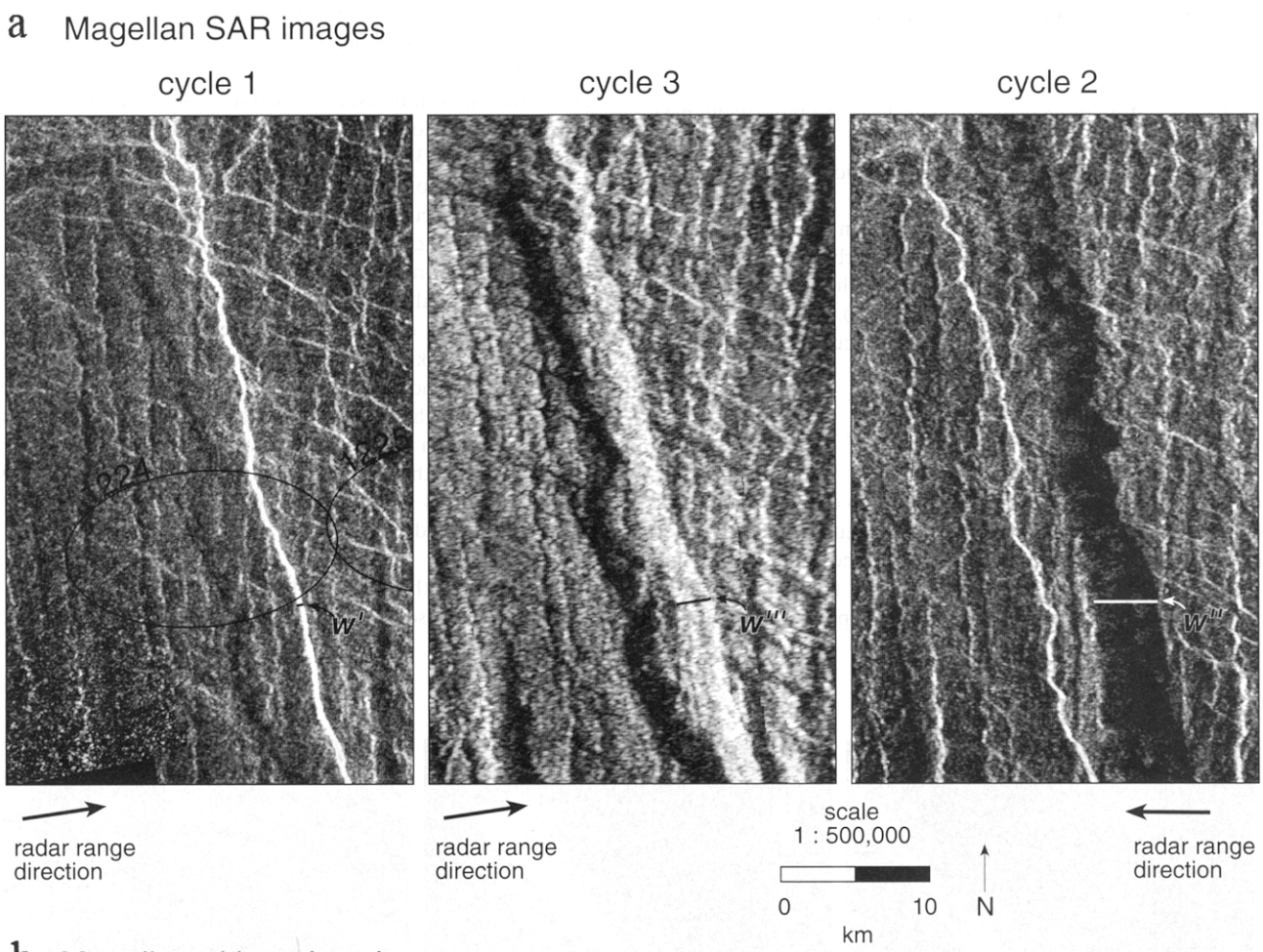

Figure 7. a) West facing surface, face A, located at about 29.5°S, 142.5° shown in three different Magellan SAR images from three different imaging cycles. Black bars in cycle 1 and 3 images indicate the width of the band of increased radar backscatter that represents the face in the left-looking images. White bar in cycle 2 image indicates the width of the band of decreased radar backscatter that represents the face in the right-looking image. Solution for the height, h = 1240 m ±224 m, and slope, α = 41.6° +5.5° / -3.5°, of the face is discussed in text. Also shown are the footprints of Magellan altimetry measurements across face A. b) The power-versus-time delay echoes for these footprints yields planetary radius values on either side of face A. The difference in these radii, h = 1262 m ±19 m, corresponds closely with the independently derived height of face A from Magellan stereo SAR.

Measurements From Cycle 2 Magellan SAR

Over most of cycle 1/3 left-looking stereo SAR coverage, an additional right-looking view of the surface was collected in cycle 2 SAR. With three viewing geometries and three width measurements, additional possible height and slope combinations may satisfy (1) - (4), but only one combination will satisfy all the appropriate equations.

Because the spacecraft receives energy in the range direction, which is normal to the azimuth direction (orbit path), width measurements must be made parallel to the range direction. Therefore these slopes determined from (1), (2), and (7) are apparent slopes in the range direction. Correction to the true topographic slope, α_{true}, can be obtained by

$$\tan \alpha_{true} = \tan \alpha / \cos \gamma \quad (8)$$

where γ is the acute angle between the dip direction of the face and the range direction of the radar, or equivalently, the acute angle between the strike of the face and the azimuth direction. Accurate range directions are available from the Magellan Notepad; however, in most cases one can approximate the range direction by looking for seams, data gaps, or repeated changes in radar brightness at swath boundaries in the images (e.g., the cycle 3 image in Figure 8). These effects are parallel to the azimuth direction, and one can measure normal to these effects to measure in the range direction. The orbit paths are slightly different between cycle 1 and 3, but these differences are small enough that the azimuth direction can be assumed to be equal for both orbits with little error occurring in the determinations of parallax. For much of the stereo coverage, the range direction in cycle 1 and 3 is 81°- 82° east of north, whereas for most of cycle 2, the range direction is essentially east-west. It should be noted that if the elevation of the crest or base of a face changes dramatically along strike, then the strike of the face in the radar image will change because of differences in the parallax of features with different heights. Because the major source of this effect with terrestrial SAR is from stream valleys in the sides of mountains, this is not a severe problem with SAR from Venus. Other phenomena however, such as cross-striking faults, can create such topography, and thus one should exercise care in determining the strike of a face.

To incorporate the additional width measurement, w'', of a west face, we first solve for the true topographic slope, α_{true}, for

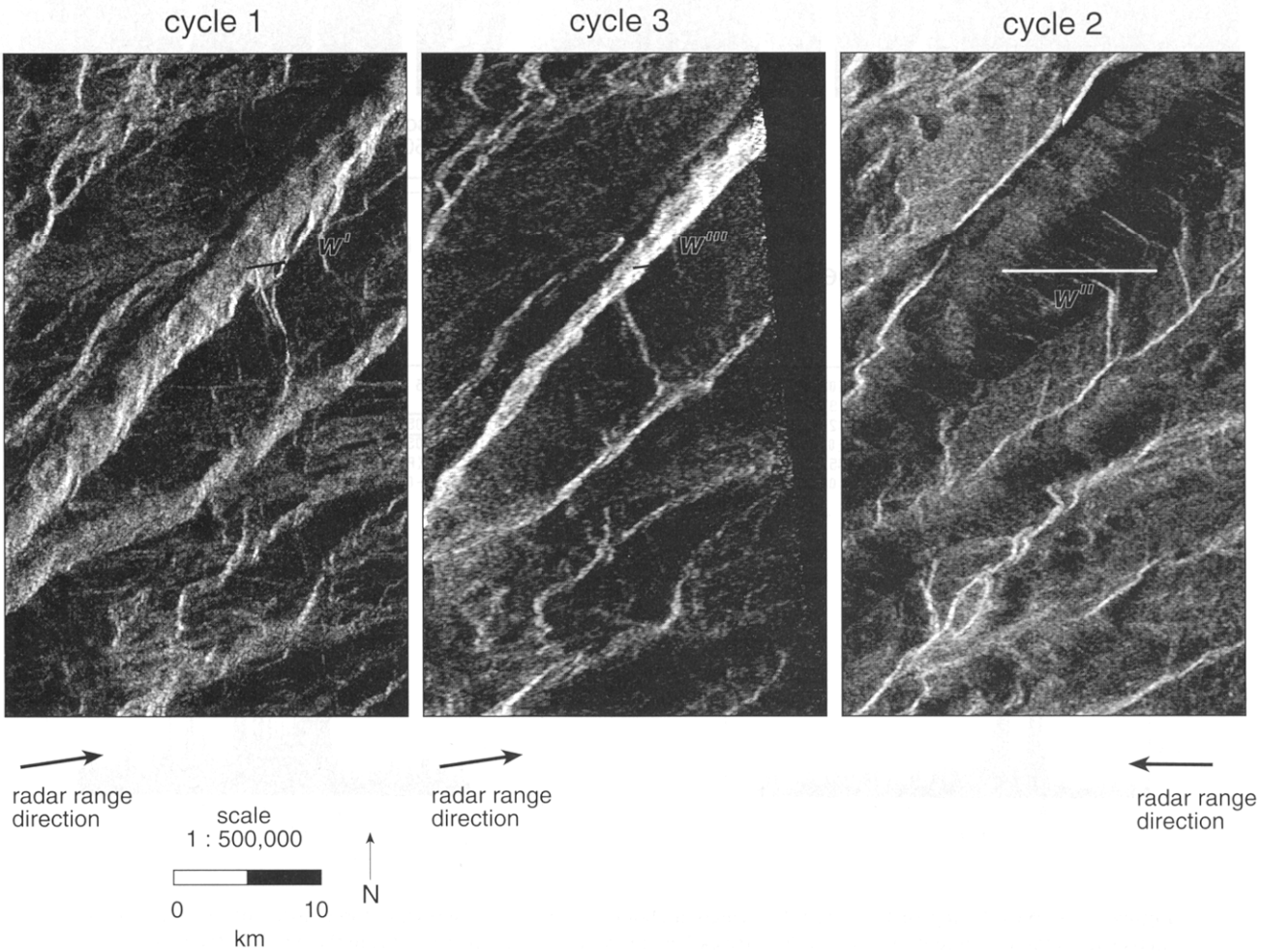

Figure 8. West facing surface, face B, located at about 18.5°S, 175° shown in three different Magellan SAR images from three different imaging cycles. Black bars in cycle 1 and 3 images indicate the width of the band of increased radar backscatter that represents the face in the left-looking images. White bar in cycle 2 image indicates the width of the band of decreased radar backscatter that represents the face in the right-looking image. Solution for the height, h = 2506 m ±216 m, and slope, α = 35.2° +1.3° / -0.7°, of the face is discussed in text.

the two α we get from the ratio w'''/w' from (7), or more easily, Figure 6a. We then calculate the two possible heights using (4); we know the parallax differences from (6). We can determine which of the relations to use in (6) because we know which two domains the face may lie in from the ratios of the widths (Figure 6).

We resolve the ambiguity by considering the width in the cycle 2 image, w''. We use the two calculated heights from (4) above and w'' to solve for the possible slopes of a west face imaged in cycle 2 using (2) and (3). We use Eqs. 2 and 3 because a west face in cycle 2 will be either elongated or in radar shadow. We then calculate the true topographic slope, α_{true}, for these slopes and compare these to the true topographic slopes we calculate from the cycle 1/3 pair. If the widths in the three images accurately measure the same discretely dipping surface, then there will be one true topographic slope that is the same in the cycle 1/3 determination and in the additional cycle 2 determination described above. Determining equivalent points in the left-looking cycle 1 and 3 and right-looking cycle 2 images sometimes requires a great deal of interpretation because the imaging is so vastly different. However, because opposite-side stereo cannot be stereoscopically fused, we feel noting changes in backscatter of a face is the best method available.

Examples

Let us return to face A in Figure 7 and try to determine the height and slope of the face with the techniques described above. The width ratio $|w'''/w'| = 5.34$ indicates that the face lies in domain 1 or 3 (see Table 1 for all calculated values). That is, the face is laid over in the cycle 3 image (as we concluded earlier), and the ambiguity lies in the nature of the face in the cycle 1 image. From Figure 6 we see that the slope in the range direction is either 29.5° if the face is foreshortened in the cycle 1 image or 41.5° if the face is laid over in the cycle 1 image. Because the strike of the face is close to the azimuth direction ($\gamma = 5°$), little correction is needed for the true topographic slope: $\alpha_{true} = 29.6°$ (for domain 1) or 41.6° (for domain 3). The two calculated heights from (4) and (6) are $h = 1810$ m (for domain 1) or 1240 m (for domain 3).

To incorporate the cycle 2 width measurement, $w'' = 4275$ m, we use the relation for elongated surfaces (2) to solve for the two predicted slopes, α, for the two possible heights calculated above. Note, because $\Omega'' = 25°$ and thus the two possible slopes are both less than 90 - Ω'', we do not need to consider the possibility that face A is in radar shadow in the cycle 2 image. For $h = 1810$ m (the domain 1 possibility), we get $\alpha = 77.9°$ ($\alpha_{true} = 78.3°$ for $\gamma = 14°$), and for $h = 1240$ m (the domain 3 possibility), we get $\alpha = 37.5°$ ($\alpha_{true} = 38.4°$). Clearly, the slope calculated with the domain 1 possibility is unreasonable, since a slope that large would be in radar shadow. Additionally this α_{true} of 78.3° does not correspond with the domain 1 α_{true} of 29.6° calculated from the cycle 1/3 images. However, domain 3 calculated slopes do correspond pretty well: $\alpha_{true} = 41.6°$ versus 38.4°. This consistency gives us confidence to conclude that face A is laid over in both cycle 1 and cycle 3 images with a topographic slope of 41.6° +5.5° / -3.5° and a height of 1240 m ±224 m. The accuracy estimates represent the theoretical maximum error based on the error in the cycle 1 and 3 width measurements. We discuss accuracy estimates in more detail in a later section.

Let us consider another example of uniquely determining the height and slope of a west facing surface. Face B in Figure 8 is not imaged as discretely as face A because an area to the west (left) of the base of the face also has high radar backscatter, but not as high as face B. This is probably due to both high surface roughness and because the area below the base of face B may

Table 1. Measurements and Calculations of Selected Surfaces on Venus

	Cycle 1 / Cycle 3 Determinations								Cycle 2 Comparisons			
Domain	$\lvert w''' \rvert$, m	$\lvert w' \rvert$, m	$\lvert w'''/w' \rvert$	dp, m	h, m	γ, deg	α, deg	α_{true}, deg	w'', m	γ, deg	α, deg	α_{true}, deg
	Face A, Location 29.5°S 142.5°, $\Omega' = 33.5°$, $\Omega''' = 17.5°$, $\Omega'' = 25.0°$											
1	2,535	475	5.34	3,010	1,812	5	29.5	29.6	4,275	14	77.9	78.3
3	2,535	475	5.34	2,060	1,240	5	41.5	41.6*	4,275	14	37.5	38.4*
	Face B, Location 18.5°S 175°, $\Omega' = 39.0°$, $\Omega''' = 20.0°$, $\Omega'' = 25.0°$											
1	1,090	2,700	0.40	3,790	2,506	53	23.0	35.2*	10,450	44	26.3	34.5*
2	1,090	2,700	0.40	1,610	1,064	53	15.0	24.0	10,450	44	7.4	10.3

	Cycle 1 / Cycle 3 Determinations								Cycle 2 Comparisons					
											Foreshortened		Laid Over	
Domain	w''', m	w', m	w'''/w'	dp, m	h, m	γ, deg	α, deg	α_{true}, deg	$\lvert w'' \rvert$, m	γ, deg	α, deg	α_{true}, deg	α, deg	α_{true}, deg
	Face C, Location 21°S 172.5°, $\Omega' = 38.0°$, $\Omega''' = 19.5°$, $\Omega'' = 25.0°$													
4	2,475	1,875	1.32	600	389	6	17.0	17.1*	400	15	17.5	18.1*	41.9	42.9
	Face D, Location 36°S 143°, $\Omega' = 30.0°$, $\Omega''' = 16.0°$, $\Omega'' = 25.0°$													
4	2,850	1,650	1.73	1,200	684	9	57.0	57.3*	1,050	0	15.2	15.2	58.7	58.7*
6	2,850	1,650	1.73	n/a	714	9	63.0	63.3	1,050	0	15.5	15.5	56.0	56.0

*Values represent compared topographic slopes used to determine domain of surface, as discussed in text. n/a, not applicable.

also be dipping toward the west, albeit at a much gentler slope. Note that the slope of the surface around face B does not affect our determination of the face itself, as long as we can still recognize separately the face from other surfaces on the three images.

Face B has a $| w''' / w' | = 0.40$, and thus the face lies in either domain 1 or 2. The face is foreshortened in the cycle 1 image; the ambiguity lies in whether the face is laid over in the cycle 3 image (domain 1) or foreshortened (domain 2). For the domain 1 possibility, $\alpha = 23.0°$, $\alpha_{true} = 35.2°$ (for $\gamma = 53°$), and $h = 2510$ m, whereas for the domain 2 possibility, $\alpha = 15.0°$, $\alpha_{true} = 24.0°$, and $h = 1060$ m (Table 1). For $w'' = 10{,}450$ m, we use the relation for elongated surfaces (Eq. 3) to solve for α for the two possible heights. We again do not need to consider the possibility that face B is in radar shadow, since $\Omega'' = 25°$ and thus $\alpha < 90 - \Omega''$. The cycle 2 image shows abundant striations, corroborating our conclusion that the face is not in radar shadow. Using the additional cycle 2 data, we calculate for the domain 1 case that $\alpha = 26.3°$ and $\alpha_{true} = 34.5°$ (for $\gamma = 44°$), and for the domain 2 case that $\alpha = 7.4°$ and $\alpha_{true} = 10.3°$. Comparing these two possible topographic slopes to those from the cycle 1/3 determinations, we see that $\alpha_{true} = 35.2°$ is much closer to $\alpha_{true} = 34.5°$ than $\alpha_{true} = 24.0°$ is to $\alpha_{true} = 10.3°$. We conclude that face B is foreshortened in the cycle 1 image but laid over in the cycle 3 image (domain 1); the topographic slope of face B is 35.2° +1.3° / -0.7°, essentially at an angle of repose, and the height is 2506 m ±216 m.

East Facing Surfaces in Magellan SAR

Extracting Topographic Slopes From Cycle 1/3 Images

Because the imaging geometries of east facing slopes are similar to west faces, we present a more condensed analysis of east faces. As with west faces, there are three distinct imaging domains for east facing surfaces in Magellan stereo radar. To avoid confusion, we use the terms domains 4, 5, and 6 for these imaging geometries. In domain 4, faces are elongated in both images; in domain, 5 faces are in radar shadow in both cycle 1 and cycle 3 images, and in domain 6, faces are elongated in the cycle 3 image and in radar shadow in cycle 1 images (Figure 9).

For east faces, we determine the topographic slope of the face, α, as we have for west faces by taking the ratio of widths of the face in the cycle 1 and cycle 3 Magellan SAR using (2) and (3) as applicable. For faces elongated in both cycle 1 and 3 images, $90 - \Omega''' > 90 - \Omega' > \alpha$ (domain 4; Figure 9b), the relation is given by

$$\frac{w'''}{w'} = \frac{\tan \Omega'(\tan \Omega''' + \tan \alpha)}{\tan \Omega'''(\tan \Omega' + \tan \alpha)} \quad (9)$$

For east faces that are in radar shadow in both cycle 1 and 3 images, $\alpha \geq 90 - \Omega''' > 90 - \Omega'$ (domain 5; Figure 9c), the ratio is given by

$$\frac{w'''}{w'} = \frac{\sin 2\Omega'}{\sin 2\Omega'''} \quad (10)$$

For faces elongated in cycle 3 images and in radar shadow in cycle 1 images, $90 - \Omega''' > \alpha \geq 90 - \Omega'$ (domain 6; Figure 9d), the ratio is given by

$$\frac{w'''}{w'} = \frac{\sin 2\Omega'(\tan \Omega''' + \tan \alpha)}{2\tan \Omega''' \tan \alpha} \quad (11)$$

The w''' / w' ratio for (9) - (11) is continuous for all α, and is plotted versus Venusian latitude for Magellan SAR for slopes $\alpha = 0°$ to $90 - \Omega'''$ in Figure 9a. For $\alpha > 90 - \Omega'''$, the relationship at $\alpha = 90 - \Omega'''$ holds, since (10) does not involve the slope of the face.

Figure 9 displays the three geometric domains of an east face, and the possible width ratios for each domain. Faces that are elongated in both cycle 1 and 3 images, domain 4, can be any value of w''' / w' from 1 through ~1.6 to ~1.8 (depending on the latitude and thus the incidence angles). The maximum value for w''' / w' is at the point where the slope is at the transition between being just imaged or just in radar shadow, $\alpha = 90 - \Omega'$. There are some higher slopes for which the ratio w''' / w' is double valued; in these cases the ratio can represent a domain 4 face and a domain 5 or a 6 face. As we discussed earlier, it is theoretically possible to determine if a face is in radar shadow by analyzing the pixel values of the imaged face. Analysis of the pixel values of both images will generally indicate the domain of the face and thus broad limits on the topographic slope. In order to determine the exact slope of the face, we make use of the w''' / w' ratio and the graph of Figure 9a. In the examples below, we make use of the cycle 2 images only to confirm our slope and height determinations.

Extracting Relative Heights From Cycle 1/3 Images

The height of a domain 4 face (Figure 9b), as with west faces, can be determined by using (4) and the parallax difference:

$$dp = w''' - w' \quad (12)$$

For domain 5 and 6 faces, one cannot use such a relation because the widths of the band of decreased backscatter are not indicative of the parallax. For a face in radar shadow the position of the right side of the band of decreased backscatter is purely a function of the incidence angle of the radar and height of the face (3). Once again, it should be noted that we are defining height of the face in this instance as the height from the crest of the face to where the shadow impinges on the surface. Given this assumption, one can use (3) for height determinations of domain 5 faces. One can use either (2) or (3) for domain 6 faces to determine the height of an east face that is in radar shadow in the cycle 1 image, but elongated in the cycle 3 image.

Examples

The east facing surface, face C, in Figure 10 is represented by the band of decreased radar backscatter in both the cycle 1 and 3 images. We determine the height and slope of the face with techniques similar to those for west faces. The width ratio $w''' / w' = 1.32$; thus Figure 9a allows us to conclude that the face is elongated and lies in domain 4 and has a topographic slope, $\alpha = 17.0°$ ($\alpha_{true} = 17.1°$ for $\gamma = 6°$). Because face C lies in domain 4, we use (4) and (12) to determine a height, $h = 390$ m for the face (Table 1).

Because face C lies in domain 4, we have unique values for the height and slope of the face. Thus we use the width of the face in the cycle 2 image simply as verification of the determinations. To incorporate the cycle 2 width measurement, $| w'' | = 400$ m, we use the relations for foreshortened and laid-over surfaces (1) to solve for two possible α for the height calculated above. If face C is foreshortened, $w'' = 400$ m, whereas if face C is laid over, $w'' = -400$ m. Since $\Omega'' = 25°$, we expect the solution for a foreshortened face in cycle 2 to be closer to our slope determination using the cycle 1/3 widths above. For the foreshortened solution, we get $\alpha = 17.5°$ ($\alpha_{true} = 18.1°$ for $\gamma = 15°$), and for the laid-over

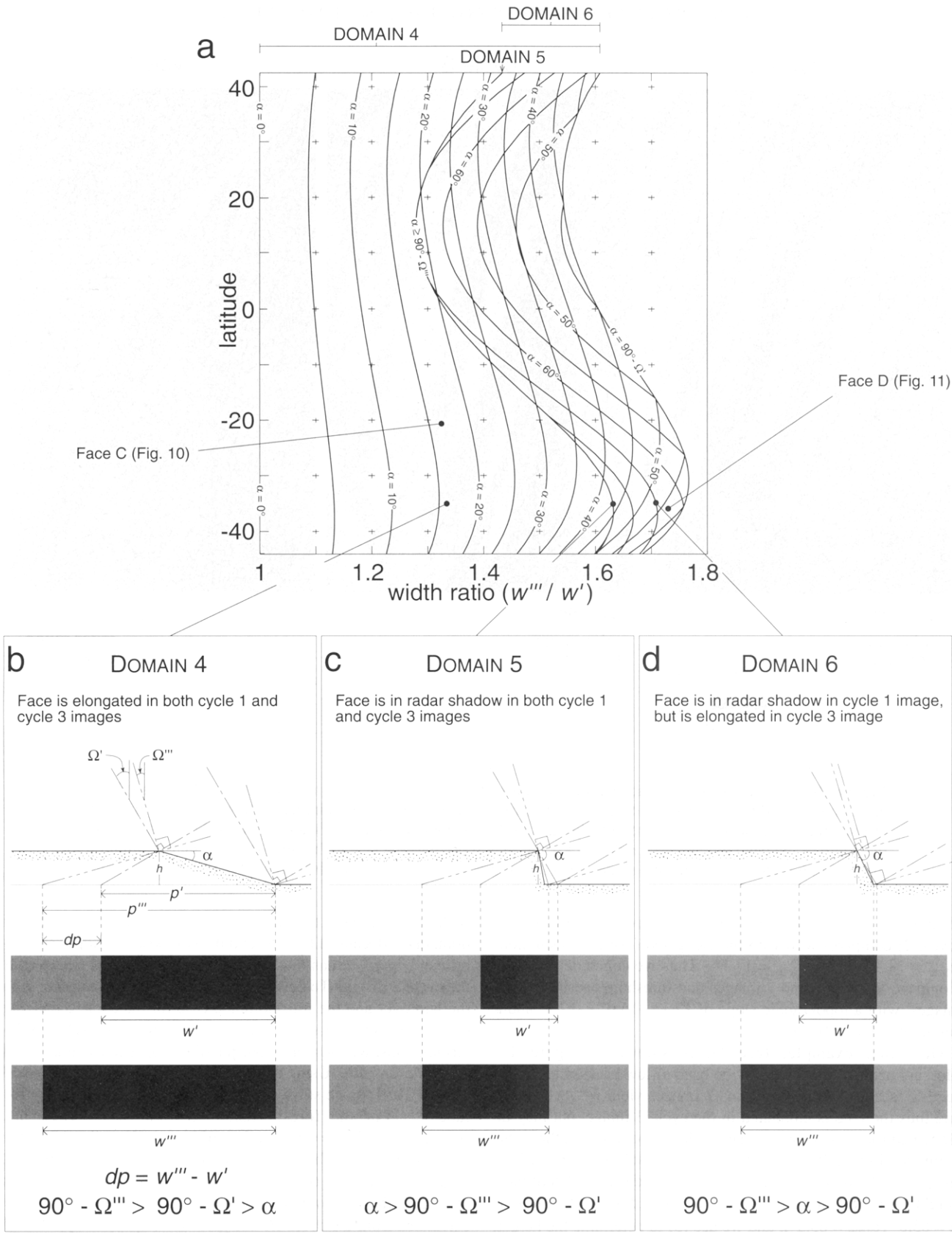

Figure 9. a) Plot of (9) - (11) for determination of the topographic slope, α, of an east facing surface from ratio of the widths, w'''/w', imaged in cycle 1 and cycle 3 Magellan SAR. Because incidence angles change with latitude in Magellan SAR (see Figure 2b), the ratio of the widths, w'''/w', is plotted versus Venusian latitude. b-d) Determination of the relative height, h, of an east facing surface from differences in the widths of the face with differing slopes in cycle 1 and 3 images. The height, h, for a surface that is elongated in both images can be determined from the parallax difference and use of (4) and (12). For surfaces that are in radar shadow, use of (3) is necessary.

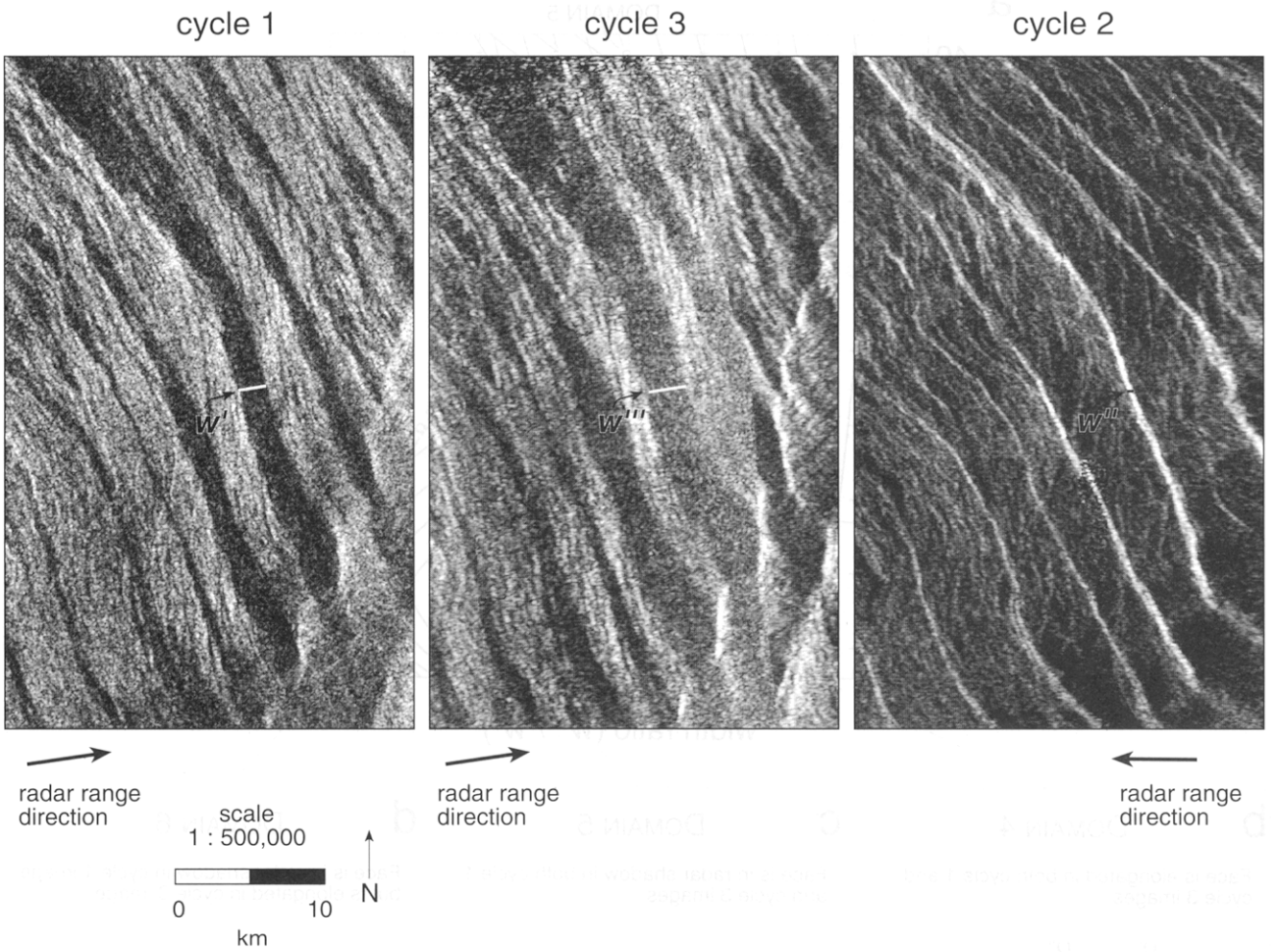

Figure 10. East facing surface, face C, located at about 21°S, 172.5° shown in three different Magellan SAR images from three different imaging cycles. White bars in cycle 1 and 3 images indicate the width of the band of decreased radar backscatter that represents the face in the left-looking images. Black bar in cycle 2 image indicates the width of the band of decreased radar backscatter that represents the face in the right-looking image. Solution for the height, h = 389 m ±217 m, and slope, α = 17.1° +15.6° / -12.1°, of the face is discussed in text.

solution, α = 41.9° (α_{true} = 42.9°). The foreshortened solution (cycle 2) compares well with the elongated (cycle 1/3) solution: α_{true} = 18.1° versus α_{true} = 17.1°. Thus we conclude face C is elongated in cycle 1 and 3 images and foreshortened in cycle 2 images, with a topographic slope of 17.1° +15.6° / -12.1° and a height of 389 m ±217 m.

Our final example, face D, is shown in Figure 11. Measurements of the widths of the band of low backscatter representing face D in the cycle 1 and 3 images yield $w'''/w' = 1.73$, and thus the face is elongated in the cycle 3 image, but may be elongated (domain 4) or in radar shadow (domain 5) in the cycle 1 image (Figure 9). For the domain 4 solution, α = 57.0° (α_{true} = 57.3° for γ = 9°), and we use (4) and (12) to determine a height, h = 680 m of the face. For the domain 5 solution, α = 63.0° (α_{true} = 63.3°), and we use (3) to determine the height, h = 710 m. Because face D is either slightly imaged (domain 4) or barely in radar shadow (domain 5), the values are close between the two cases.

Analysis of pixels indicate very low values of normalized backscatter cross section (< -8 dB in places), but these values are higher than the background noise level of Magellan for this part of the image (-10 dB). Thus we conclude that the face is not in radar shadow and is imaged by the radar. We will use the cycle 2 width measurement to confirm that the face does indeed fall in domain 4. Because Ω'' = 25° and the two possible slopes are significantly greater than that, we suspect that face D is laid over in the cycle 2 image. To be thorough, we nonetheless consider both the laid over and the foreshortened case for the cycle 2 imaging of face D. Because we have two heights from the cycle 1/3 determinations, we thus have four possible slopes to calculate from the cycle 2 width. Using the heights, h = 680 m and 710 m, and $|w''|$ = 1050 m, we solve for the slope using (1) as we have for face C. For the foreshortened solution (w'' = 1050 m), $\alpha = \alpha_{true}$ = 15.2° (γ = 0°) for h = 680 m, and α_{true} = 15.5° for h = 710 m. For the laid over solution (w'' = -1050 m), α_{true} = 58.7° for h = 680 m, and α_{true} = 56.0° for h = 710 m. As we expect the laid over solution slopes are much closer to those calculated from the cycle 1/3 images. More specifically, the laid over solution for h = 680 m (domain 4) is closer to the cycle 1/3 calculation: α_{true} = 58.7° versus α_{true} = 57.3°, than is the laid over solution for h = 710 m (domain 5): α_{true} = 63.3° versus α_{true} = 56.0°. Thus we conclude that face D is elongated in both the cycle 1 and 3 images (domain 4) and that it is laid over in the cycle 2 image. The topographic slope for face D is 57.3° +3.0° / –32.6°, probably indicative of the primary fault-scarp geometry, and the height of the face is 684 m ±232 m.

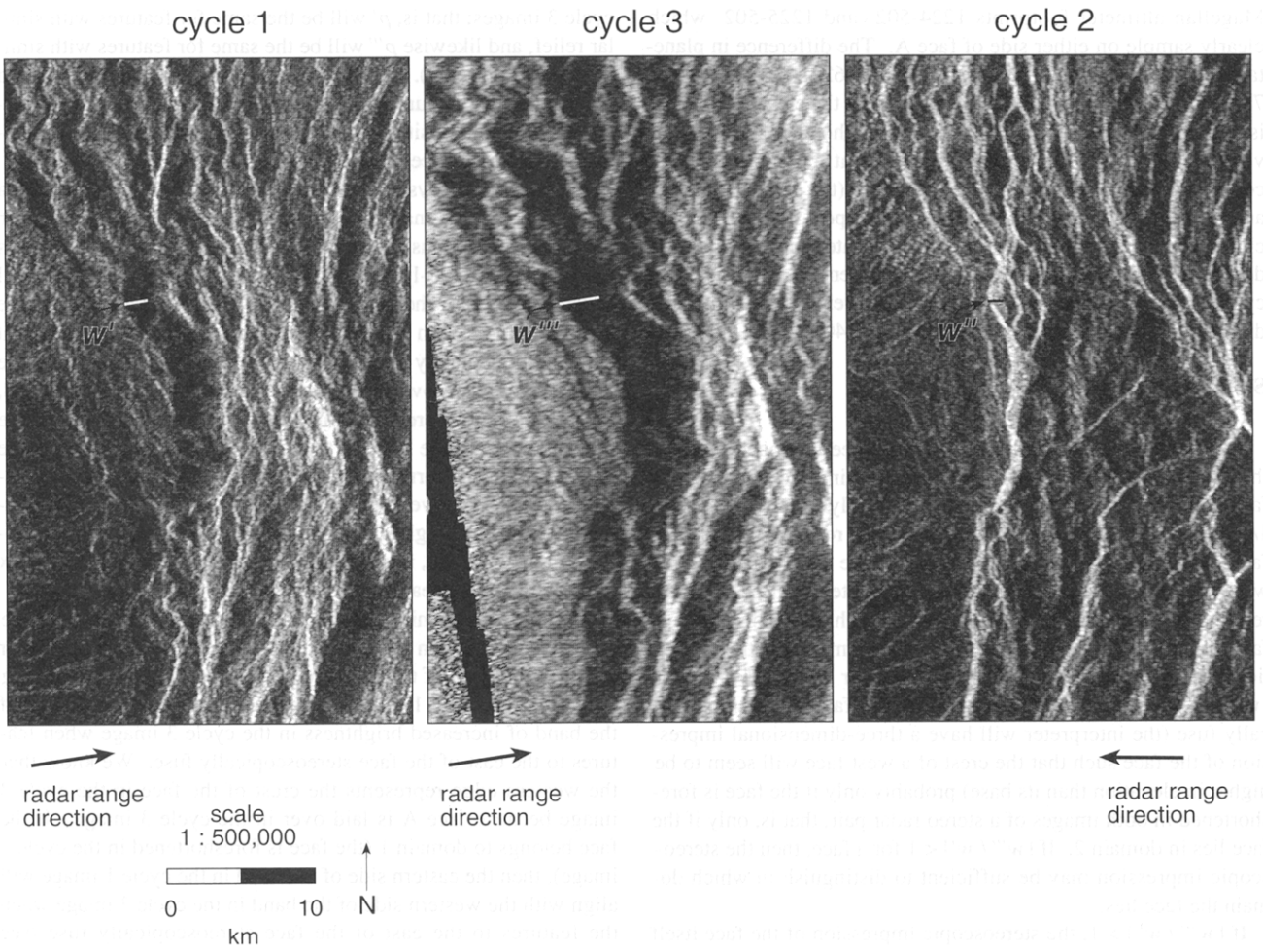

Figure 11. West facing surface, face D, located at about 36°S, 143° shown in three different Magellan SAR images from three different imaging cycles. White bars in cycle 1 and 3 images indicate the width of the band of decreased radar backscatter that represents the face in the left-looking images. Black bar in cycle 2 image indicates the width of the band of decreased radar backscatter that represents the face in the right-looking image. Solution for the height, h = 684 m ±232 m, and slope, α = 57.3° +3.0° / -32.6°, of the face is discussed in text.

Other Information Aiding Unique Determination

In cases where a west facing surface is imaged well in all three cycles, we believe the incorporation of cycle 2 images is the most effective method of unambiguously determining the height and slope of the face; however, use of cycle 2 images may not always be desirable or possible. For example, the face may not have been imaged in cycle 2, or there may be other effects contributing to radar backscatter, such as surface roughness, that lessen the ability to recognize a discretely dipping surface in cycle 2. As stated above, because the distortions in opposite-side radar are so great, it is often difficult to detect an equivalent feature, such as the base or crest of a face in both left-looking cycle 1/3 and right-looking cycle 2 Magellan SAR. We describe below two other methods that may help determine the domain of a face.

Magellan Altimetric Echoes

Recall that with cycle 1/3 Magellan SAR we are usually left with two possible imaging domains that satisfy width measurements in the two images. When confronted with two possible heights derived from (4), one can compare these calculated heights with the height extracted from Magellan altimetric measurements of power-versus-time delay echoes. These are the original data that are then gridded to construct the global topographic data for Venus, such as that shown in Figure 1. A thorough explanation of these data can be found in the work by *Ford and Pettengill* [1992]. These echoes have footprint resolutions generally greater than 10 km in both the azimuth and range directions, and thus it is often difficult to distinguish which portion of the surface is contributing most to the altimetry signal. But in some cases the positions of the footprints may be such that the surface is clearly sampled by different echoes on either side of the face of interest. The difference in the elevations of two such echoes may correspond closely to one of the two heights determined through (4), and thus provide independent information as to which domain the face lies in. Note that the elevation difference by this method will probably not exactly match the calculated heights unless the surface is flat on either side of the face and the entire elevation change between echoes is due to the face itself. But exact matches are not required if we are using these echoes to distinguish between domains.

Note from our analysis of face A of just the cycle 1 and 3 SAR images, we calculated that face A had a height, h = 1810 m (for domain 1) or 1240 m (for domain 3). Shown in Figure 7a are

Magellan altimeter footprints 1224-502 and 1225-502 which clearly sample on either side of face A. The difference in planetary radii between these two footprints is 1262 m ± 19 m (Figure 7b). If we make the assumption that most of the elevation change is due to the face, then the height of face A should be close to this value. Analysis of the images suggests that there is little other contribution to the elevation across this face (the areas to the west and east of the face appear to have low slopes), and so we conclude that Magellan altimetry echoes indicate that face A lies in domain 3. This is consistent with our independent analysis of the cycle 2 image, which indicates that the lower height is more indicative of the height of the face with $h = 1240$ m ±224 m.

Stereoscopic Impression

Although the most qualitative of the three approaches, using the stereoscopic impression to help determine the domain of a face can always be attempted because it only requires the cycle 1/3 stereo pair. Our explanation here will be restricted to surfaces facing the antenna, but the strategy can be easily modified to work with surfaces facing away from the antenna. Recall that to resolve the ambiguity of the calculated height and slope for surfaces facing the antenna, one needs to determine whether a face lies in domain 1 or 2 (for $|w'''/w'| < 1$) or domain 1 or 3 (for $|w'''/w'| > 1$). As we have stated above, a face will stereoscopically fuse (the interpreter will have a three-dimensional impression of the face such that the crest of a west face will seem to be higher in elevation than its base) probably only if the face is foreshortened in both images of a stereo radar pair, that is, only if the face lies in domain 2. If $|w'''/w'| < 1$ for a face, then the stereoscopic impression may be sufficient to distinguish in which domain the face lies.

If $|w'''/w'| > 1$, the stereoscopic impression of the face itself will not yield information to help determine the domain, and the stereoscopic impression of features around the face may be more useful. The task is to determine another feature that has the same height, and therefore differential parallax, as the crest or base of the face of interest. This technique is applicable because features with similar relief, h, above the topography model will have similar distortions in the positions of these features in the cycle 1 and cycle 3 images; that is, p' will be the same for features with similar relief, and likewise p''' will be the same for features with similar relief (Figure 12). If the topography model is nondipping and planar between features (a valid assumption only over small distances), relative positions of features with similar relief will remain constant between cycle 1 and cycle 3 images.

Because we always know the position of the crest and base of a face in one of the images, one applies the technique to solve for the other, ambiguous image. The technique works best in areas that have some flat-lying regions away from the face. We will consider the case where $|w'''/w'| > 1$, but the technique can be applied to faces with $|w'''/w'| < 1$ just as easily. We noted that one can immediately determine that face A in the cycle 3 image of Figure 7 is laid over because $|w'''/w'| > 1$, and as expected, the face does not stereoscopically fuse properly. However, subtle relief features to the west of the face (in the hanging wall if the face represents a normal fault scarp) and to the east (in the footwall) do fuse relatively well. If the crest of the face is approximately the same height above the topography model as these features in the footwall, it will have approximately the same parallax as these features in each of the images.

In order to determine the crest of face A in the cycle 1 image (and thus the domain of the face), we look for which edge (left or right) of the band of the increased radar backscatter representing face A in the cycle 1 image correlates with the western edge of the band of increased brightness in the cycle 3 image when features to the east of the face stereoscopically fuse. We know that the western edge represents the crest of the face in the cycle 3 image because face A is laid over in the cycle 3 image. If the face belongs to domain 1 (the face is foreshortened in the cycle 1 image), then the eastern side of the band in the cycle 1 image will align with the western side of the band in the cycle 3 image when the features to the east of the face stereoscopically fuse (see Figure 6b). Likewise, if the face belongs to domain 3 (the face is laid over in the cycle 1 image), then the western side of the band in the cycle 1 image will align with the western side of the band in the cycle 3 image (see Figure 6d). A similar analysis could be carried out that coupled the eastern side of the band in the cycle 3 image (the base of the face) and subtle features to the west of the face.

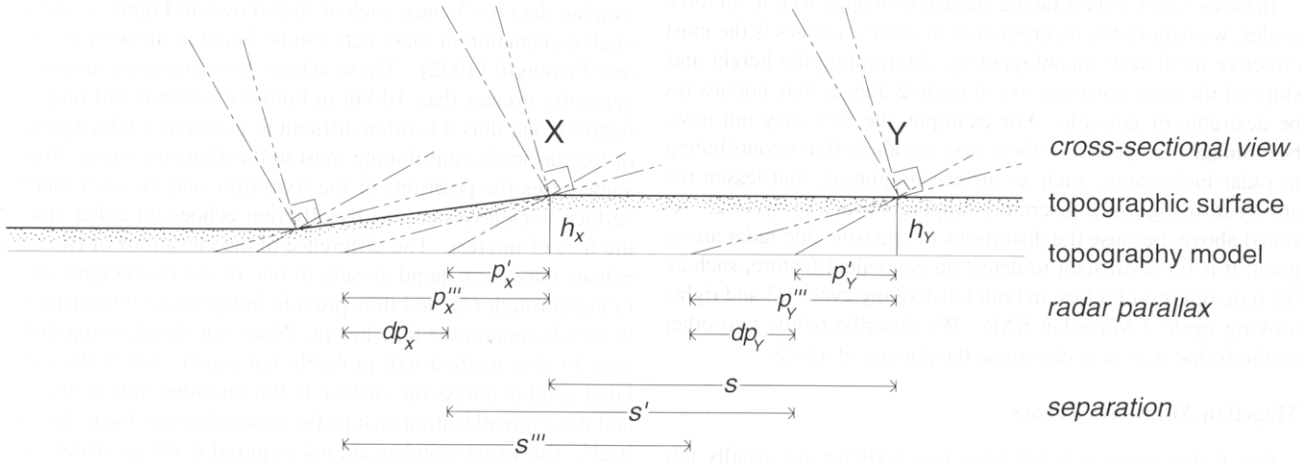

Figure 12. Features, X and Y, with similar relief, $h_X = h_Y$, above the topography model will have similar parallaxes, p' and p''', and thus parallax differences, $dp_X = dp_Y$. This means the relative positions of these features will remain constant between cycle 1 and cycle 3 images, i.e., the separation, $s = s' = s'''$. Thus even if one cannot stereoscopically fuse X, one can determine dp_X by determining dp_Y through stereoscopic fusion of Y.

This method of distinguishing between domains can be difficult unless one has access to a stereoplotter, such as the soft-copy system available in the Magellan Stereo Toolkit, to interactively clear the parallax for subtle relief features. We have studied the stereoscopic impression of the images in Figure 7 with this system and have come to the same conclusion as we did for the method using cycle 2 widths, namely, that the western side of the band of increased brightness in the cycle 1 image is the crest of the face, and therefore the face is laid over in the cycle 1 image also.

It should be noted that we are not arguing that the entire footwall has exactly the same parallax difference. We are saying that parallax differences are close enough to being the same that they can be distinguished from other large parallax differences, such as those in the hanging wall to the west of face A. Recall that this is all that is needed to distinguish between two domains. We can determine the exact height and slope of a face with (4) and (7) once we know in which domain the face lies.

Augmenting Digital Elevation Model Generation

If one is interested in heights and slopes of discretely dipping surfaces, then the simple techniques presented in this report may be the preferred method, but the techniques in no way supplant traditional stereo radargrammetry. If one has access to a stereoplotter, a skilled operator and an accurate knowledge of the topography model, then one may wish to construct digital elevation models (DEMs) to quantify the shape of a planet's surface because the process of stereoscopic fusion may be more accurate then attempting to determine equivalent points by changes in radar backscatter of a face. Furthermore in areas that do not have discrete faces, the stereoscopic impression may still be quite good. However, in areas where layover or radar shadow are present, and thus one cannot stereoscopically fuse a feature, one can augment DEM construction as follows.

In cases where a surface is laid over or in radar shadow, the task is still just to determine the radar parallax. The methods described in the previous section can be applied here. Essentially one uses the stereoscopic impression of everything around the face, but not of the face itself, since the face will not properly fuse, as a guide to the true parallax difference of a face. One attempts to determine equivalent points in an image pair by fusing features that one suspects have a similar parallax as the base or crest of the face of interest. One then looks for the correspondence of positions of the edges of the face in each image, knowing for which parallax one has cleared, and thus which features are of correlative parallax. For example, in the case of face A (Figure 7), one would collect points along the left side of the band of increased brightness in both cycle 1 and 3 images when these sides are aligned to get the parallax of the crest of the face (see Figure 6d for the parallaxes of a domain 3 face). The measured parallax difference will be correct even though the collected points may overlap other points such as those for the base of the face.

Accuracy of Heights and Slopes

The accuracy of the heights and slopes determined using the method presented here is a function of the accuracy of the width measurements from the cycle 1 and 3 images. Each width measurement has a total uncertainty of ±1 range resolution, Ry, because each end of the linear measurement has a position uncertainty of ±0.5 R_y. The range resolution is described by

$$R_y = c \,/\, 2B \sin \Omega \tag{13}$$

where c is the speed of light, B is the effective bandwidth, and Ω is the incidence angle [*Moore,* 1983]. *Sanders et al.*, [1992] reported R_y values for cycle 1 Magellan SAR, but no cycle 3 resolutions have been reported. The effective bandwidth, however, is thought to have remained constant throughout the Magellan mission (*W. Johnson,* personal communication, 1995), and thus cycle 3 range resolutions, R_y''', are equivalent to cycle 1 range resolutions, R_y', at comparable incidence angles. Note $R_y''' \neq R_y'$ at the same latitude because $\Omega' \neq \Omega'''$ at a given latitude (Figure 2). Alternatively R_y''' can be calculated by using B = 2.07 s^{-1} in Eq. 13; this is the approximate value for effective bandwidth that *Sanders et al.*, [1992] used for their R_y' determinations.

For the cycle 1 width measurement, w', we denote the measurement uncertainty by $dw' = \pm 1R_y'$. Likewise we call $dw''' = \pm 1R_y'''$ the measurement uncertainty for w'''. Substituting these into (4), the height uncertainty, dh, is given by

$$dh = (dw' + dw''') \,/\, (\cot \Omega''' - \cot \Omega') \tag{14}$$

To solve for uncertainties in slope determinations, $d\alpha$, we cannot directly substitute dw' and dw''' into (7) and (9) because these equations are nonlinear with respect to α. Likewise, $d\alpha$ is asymmetric about α, and thus $+d\alpha \neq |-d\alpha|$. However we can solve for the maximum slope, $\alpha_{max} = \alpha + d\alpha$, through

$$\frac{w''' + dw'''}{w' - dw'} = \frac{\tan \Omega'(\tan \Omega''' - \tan \alpha_{max})}{\tan \Omega'''(\tan \Omega' - \tan \alpha_{max})} \qquad w'''/w' < 0$$

$$\frac{w''' - dw'''}{w' + dw'} = \frac{\tan \Omega'(\tan \Omega''' - \tan \alpha_{max})}{\tan \Omega'''(\tan \Omega' - \tan \alpha_{max})} \qquad w'''/w' > 0 \tag{15}$$

In using (15), and also in (16) below, the sign of a width measurement uncertainty should be taken to be the same as the sign of the width measurement. For example, if a face lies in domain 1, then both w''' and dw''' are negative. The left side of (15) yields a ratio that can be used with the graph on Figure 6a to yield α_{max}. Correction to true maximum slope, $\alpha_{true_{max}}$, is necessary and can be obtained through Eq. 8. Finally the positive, true slope uncertainty can be determined by $+d\alpha_{true} = \alpha_{true_{max}} - \alpha_{true}$. To solve for the minimum slope, $\alpha_{min} = \alpha - d\alpha$, we use

$$\frac{w''' - dw'''}{w' + dw'} = \frac{\tan \Omega'(\tan \Omega''' - \tan \alpha_{min})}{\tan \Omega'''(\tan \Omega' - \tan \alpha_{min})} \qquad w'''/w' < 0$$

$$\frac{w''' + dw'''}{w' - dw'} = \frac{\tan \Omega'(\tan \Omega''' - \tan \alpha_{min})}{\tan \Omega'''(\tan \Omega' - \tan \alpha_{min})} \qquad w'''/w' > 0 \tag{16}$$

and the negative, true slope uncertainty is determined by $-d\alpha_{true} = \alpha_{true_{min}} - \alpha_{true}$. A similar approach for east facing surfaces (domains 4 through 6) can be derived to solve for the uncertainty in these slope determinations. For example, for domain 4 faces, changing signs on the right side of (15) will suffice. In the interest of brevity, we present only the results of the uncertainty analysis relevant to east facing surfaces (faces C and D) analyzed in this report.

Inspection of Table 2 indicates that for surfaces analyzed in this report, relative uncertainties are much lower for west facing surfaces (faces A and B). Because height uncertainties are only a function of incidence angle (14), absolute height uncertainties are similar for different faces, resulting in larger heights having lower relative uncertainties. Thus the smaller relative height uncertain-

Table 2. Accuracy of Height and Slope Determinations

	h, m	dh, m	α_{true}, deg	$+d\alpha_{true}$, deg	$-d\alpha_{true}$, deg
Face A	1,240	224	41.6	5.5	3.5
Face B	2,506	216	35.2	1.3	0.7
Face C	389	217	17.1	15.6	12.1
Face D	684	232	57.3	3.0	32.6

ties of faces A and B occur simply because their heights are larger than those of faces C and D.

Slope uncertainties, however, vary greatly, depending on the orientation of the face relative to the antenna. Inspection of Figures 6a and 9a reveals that slopes are much less sensitive to uncertainties in the w'''/w' ratio for west facing surfaces. For example, a difference of ~50% in the w'''/w' ratio for east facing surfaces spans almost the entire range of possible slope values, whereas this same change in w'''/w' for west facing surfaces has a much smaller effect on the slope determination. This is a beneficial result because the method presented here has its most important application in laid-over surfaces. Additionally, most east facing surfaces on Venus fall in domain 4 and thus slopes can be obtained through radar stereoscopy.

With this accuracy analysis, we have determined the theoretical maximum error if both the cycle 1 and 3 width measurements are in error ±1 full R_y from their true widths. Independent cycle 2 width measurements (Table 1) and altimetry echoes (Figure 7), which closely agree with our height and slope determinations from cycle 1 and 3 images, suggest that these uncertainty estimates may be excessive in some cases, such as with faces C and D. This may be because we are measuring widths of features that are laterally much more extensive than their widths, and thus these widths are generally more easily recognizable from background in the image than theoretical resolution estimates might indicate. One reason for this may be that the along-strike character of the edge contributes to the interpretation of the edge of the feature at the measurement location. In addition, R_y does not take into account the multiple-look summation of SAR, which tends to decrease radar speckle in SAR, and thus increase the quality of the images. This is even more relevant for Magellan SAR, where the maximum number of looks occurs at high latitudes, where R_y is poorest, thus somewhat offsetting the lower resolution at these latitudes [*Pettengill et al.,* 1991].

Conclusions

In areas of steep terrain, a radar stereo pair may be insufficient to uniquely determine the height and slope of a discretely dipping surface. In this report we developed relationships that allow one to measure the relative heights and slopes of surfaces in steep terrain, by sorting out the different distortions of radar layover, shadow, foreshortening and elongation in radar images. We applied the techniques to Magellan stereo SAR images of the planet Venus although the methods can be used on any stereo radar data set if the radar incidence angles are known.

The methods make use of the widths of a band of increased or decreased radar backscatter relative to flat-lying features that represent a discretely dipping surface, and thus do not require the ability to stereoscopically fuse a surface. Differences in the widths of these bands in the cycle 1 and 3 images allow one to determine the height of a face, whereas the ratio of the widths enables one to determine the topographic slope.

We showed that with only two imaging geometries, there is generally an ambiguity of two possible relative heights and slopes of a surface, and presented techniques that incorporate additional data to relieve this ambiguity. These can take the form of an additional SAR image, additional height or slope information from independent sources, or in some cases, a consideration of the stereoscopic impression of a face or features around a face. Because right-looking cycle 2 Magellan SAR was collected over most of the same regions as left-looking cycle 1/3 stereo Magellan SAR, we primarily employed additional width measurements from cycle 2 images in this report to resolve imaging ambiguities of the examples presented.

With these methods, we showed that discretely dipping surfaces on Venus can have topographic slopes close to 60° with heights in the 700 m range. Because the surface of Venus has undergone little large-scale erosion, we believe slopes of this magnitude most likely represent primary normal-fault scarp orientations. Retention of primary fault scarps of this steepness and with this much relief suggests a high effective cohesive strength to the Venusian crust. Surfaces display a wide variety of lower slopes with heights of at least 2500 m, consistent with other high-resolution determinations of topographic slopes on Venus [*Ford and Pettengill*, 1992; *Leberl et al.,* 1992]. Surfaces in this slope range analyzed in this report most likely represent scree slopes or fault scarps that have experienced rotation through subsequent deformation.

Acknowledgments. This work is supported in part by the Guest Investigator Program of the Magellan Project, NASA-JPL contract 958940, and the Venus Data Analysis Program, NASA-LPI contract NAGW-3706. John Suppe, Jeff Moore and Franz Leberl provided careful reviews of the manuscript. Franz Leberl also answered many of my radar stereo questions. Karl Mueller and Maribeth Price reviewed an earlier version of the manuscript, and Frank Bilotti, Jay Lieske, and Fred Suppe provided helpful comments. Kathryn Sasowsky, Allan Rubin, and Tullis Onstott provided helpful comments about accuracy estimates. Peter Ford was very knowledgeable and patient with explanations regarding Magellan data and radar in general. I am also thankful for his and Fang Liu's excellent Magellan-related software. Susan Slavney and Jeff Plaut were very helpful with sorting out Magellan data products. Kelly Maurice explained the Magellan Stereo Toolkit to me and debugged it for our system (for additional information on the Magellan Stereo Toolkit, contact Kelly Maurice at Vexcel Corporation, 55th St. Boulder, CO 80301).

References

Ardvidson, R. E., R. Greeley, M. C. Malin, R. S. Sanders, N. Izenberg, J. J. Plaut, E. R. Stofan, and M. K. Shepard, Surface modification of Venus as inferred from Magellan observations of plains, *J. Geophys. Res.*, *97*, 13,303-13,318, 1992.

Dalke, G. W., and R. M. McCoy, Regional slopes with non-stereo radar, *Photogramm. Eng.*, *XXIV*, 446-452, 1968.

Ford, P. G., and G. H. Pettengill, Venus topography and kilometer-scale slopes, *J. Geophys. Res.*, *97*, 13,103-13,114, 1992.

Fullerton, K., F. Leberl, and R. Marque, Opposite side sar image processing for stereo viewing, *Photgramm. Eng.*, *LII*, 1487-1498, 1986.

Greeley, R., et al., Aeolian features on Venus: preliminary Magellan results, *J. Geophys. Res.*, *97*, 13,319-13,346, 1992.

Head, J. W., L. Crumpler, J. Aubele, J. Guest, and R. S. Sanders, Venus volcanism: classification of volcanic features and structures, associations, and global distribution from Magellan data, *J. Geophys. Res.*, *97*, 13,153-13,198, 1992.

Klose, K. B., J. A. Wood, and A. Hashimoto, Mineral equilibria and the high radar reflectivity of Venus mountaintops, *J. Geophys. Res.*, *97*, 16,353-16,369, 1992.

LaPrade, G., Stereoscopy, in *Manual of Photogrammetry*, edited by C. C. Slama, pp. 519-544, American Society of Photogrammetry and Remote Sensing, Bethesda, Md., 1980.

Leberl, F. W., *Radargrammetric Image Processing*, Artech House, Norwood, Mass., 1990.

Leberl, F. W., J. K. Thomas, and K. E. Maurice, Initial results from the Magellan stereo experiment, *J. Geophys. Res.*, *97*, 13,675-13,689, 1992.

Kaula, W. M., Venus: A contrast in evolution to Earth, *Science, 247*, 1191-1196, 1990.

Malin, M. C., Mass movements on Venus: preliminary results from Magellan cycle 1 observations, *J. Geophys. Res.*, *97*, 16,337-16,352, 1992.

Moore, R. K., Imaging radar systems, in *Manual of Remote Sensing*, edited by R. N. Colwell, pp. 429-474, American Society of Photogrammetry and Remote Sensing, Bethesda, Md., 1983.

Muhleman, D. O., Radar scattering from Venus and the Moon, *Astron. J.*, *69*, 34-41, 1964.

Pettengill, G. H., P. G. Ford, W. T. K. Johnson, K. Raney, and L. A. Soderblom, Magellan: Radar performance and data products, *Science*, *252*, 260-265, 1991.

Plaut, J. J., Stereo imaging, in *Guide to Magellan Image Interpretation*, edited by J. P. Ford, J. J. Plaut, C. M. Weitz, T. B. Farr, D. A. Senske, E. R. Stofan, G. Micheals, and T. J. Parker, pp. 33-43, Jet Propul. Lab., Pasadena, Calif., 1993.

Sanders, R. S., et al., Magellan mission summary, *J. Geophys. Res.*, *97*, 13,067-13,090, 1992.

Wu, S. S. C., The solution of the layover problem of side-looking radar images, in *Reports of Planetary Geology Program-1982*, edited by H. E. Holt, pp. 370-372, NASA, Washington, D. C., 1982.

C. Connors, Department of Geological and Geophysical Sciences, Princeton University, Princeton NJ 08544-1003. (e-mail: chris@wanda.princeton.edu)

(Received June 21, 1994; revised April 4, 1995;
accepted April 5, 1995.)